PALACKÝ UNIVERSITY OLOMOUC

Faculty of Science

Department of Physical Chemistry

Master's thesis

Hybrid Nanomaterials based on Graphene and their Application in Electrochemistry

Anna Stuchlá

Supervisor:	Ing. Veronika Urbanová, Ph.D.
Study program:	N1407 Chemistry
Study course:	Material Chemistry
Form of study:	Daily attendance

Olomouc 2018

Declaration of the author

I declare that I have worked out this thesis by myself under supervision of Ing. Veronika Urbanová, Ph.D. All references and information sources used in this thesis are properly cited.

I agree with the accessibility of my thesis in the library of Physical Chemistry Department, Faculty of Science, Palacký University in Olomouc.

Olomouc, April 2018 ……

Anna Stuchlá

Acknowledgement

There are a number of people who have contributed to make this thesis done and to whom I would like to greatly thank. At first I thank my supervisor Veronika Urbanová for her professional advice, patience and devoted time through whole area of working and testing the electrochemical nature of graphene-doped materials.

Sincerely, I would like to thank to Regional Center of Advanced Technologies and Materials and Department of Physical Chemistry for facilitating of my work and to all its employees who helped me with measuring and understanding various analyses and techniques, individually Dr. C. Aparicio for measuring the XRD patterns of all my samples, Dr. V. Ranc for measuring Raman spectroscopy, Mgr. J. Stráská and Mgr. C. Pérez for providing me TEM and SEM analyses. Many thanks also belong to Mgr. M. Petr for XPS analysis.

My great thanks belong to my family for the support in the study.

Bibliographical identification

Author´s first name and surname:	Anna Stuchlá
Title:	Hybrid Nanomaterials based on graphene and their application in electrochemistry
Department:	Department of Physical Chemistry
Type of thesis:	Master´s
Supervisor:	Ing. Veronika Urbanová, Ph.D
The year of presentation:	2018

Abstract

Due to poor kinetics of oxygen reduction reaction (ORR) occurring in fuel cells, current research has focused to metal-free nitrogen-doped graphene catalysts that are environmentally friendly and cost-effective. The most promising nitrogen configurations contributing to enhanced catalytic activities are pyridinic, graphitic and pyrrolic nitrogen, however, their individual effects and controllable synthesis is hardly achieved. The aim of this work was to control the synthesis of nitrogen-doped graphene aerogels (GA-N) via cost-effective, facile and large-scale hydrothermal method to obtain various types of incorporated nitrogen. This was achieved by variable reaction conditions such as type of nitrogen precursor and ratio between GO and nitrogen precursor. All samples were characterized by spectroscopic and microscopic techniques and tested for electro-chemical behavior and ORR catalysis. The ORR activities in terms of electrochemical response, onset potential and current density have been compared with type of nitrogen configuration incorporated within the graphene lattice. According to the results obtained in this thesis, the highest electro-catalytic response toward ORR showed catalyst that was synthetized using ethylenediamine as nitrogen precursor. The sample revealed pyridinic and pyrrolic nitrogen configuration and exhibited enhanced catalytic activities toward ORR in alkaline, neutral and also acidic media.

Key words:	Oxygen reduction reaction, electro-catalysis, graphene, graphene oxide, nitrogen doping, aerogels.
Number of pages:	68
Language:	English

List of Abbreviations

GO – Graphene oxide

rGO – Reduced graphne oxide

GA – Graphene aerogel

GH – Graphene hydrogel

GA-N – Nitrogen doped graphene aerogel

EDA – Ethylenediamine

PVP – Poly(vinyl)pyrrolidone

pPDA – *Para*-phenylenediamine

ORR – Oxygen reduction reaction

HER – Hydrogen evolution reaction

XRD – X-ray diffraction

SEM – Scanning electron microscopy

TEM – Transmission electron microscopy

FT-IR – Fourier transform infra-red spectroscopy

XPS – X-ray photoelectron spectroscopy

CV – Cyclic voltammetry

EIS – Electrochemical impedance spectroscopy

LSV – Linear sweep voltammetry

GCE – Glassy carbon electrode

RDE – Rotating disc electrode

RRDE – Rotating ring disc electrode

PBS – Phosphate buffer solution

Contents

1. Introduction

Recently, research in the field of fuel cells has become attractive from the scientific and ecological point of view. The alarming searching for efficient alternative to currently used fossil fuels applied in combustion motors in cars rises from the depletion of earth´s fossil fuels as well as from increasing pollution and climate change caused by release of combustion waste to the air[1]. Fuel cell is an electrochemical cell that converts the chemical energy of a fuel into electrical energy through an electrochemical reaction[1]. Such environmentally friendly technology is believed to replace the combustion engines in near future[2,3].

Generally, to participate in the electrochemical reaction, fuel cells require a fuel that is oxidized at the anode and oxidizing agent that is reduced at the cathode. The weak point of this environmentally friendly solution is poor kinetics of the oxygen reduction reaction (ORR) that occurs at the cathode. ORR efficient performance is commonly facilitated via catalyst deposited at the cathode surface. Initially, ORR catalyst were based on platinum, however the high cost and low platinum sources let to platinum alloys or other noble-based catalysts and their composites. Nevertheless, request for low-cost and environmentally friendly catalyst persisted and research has focused as well on metal-free catalysts.

Recently, scientific interest has focused to carbon-based materials. They are materials capable of high adsorption capabilities, possessing high surface areas and their electronic properties could be easily tailored via suitable functionalization. Very suitable has appeared graphene-based materials, which can be doped with heteroatom such as nitrogen, sulfur, boron or phosphorus to tune the electronic properties by band gap modification. In this context, nitrogen doping has shown positive impact to ORR efficiency. Nitrogen atoms incorporated into graphene network contribute with free electron pair to the aromatic conjugation which enables faster electron transfer, opens the band gap and thus increases electrical conductivity. Foremost, nitrogen modulates charge distribution and spin density on the adjacent C atoms, which thus creates active sites for ORR catalysis. Recent studies demonstrated high resistance to CO poisoning and long-term stability of N-doped graphene catalyst during fuel cell operation. Nitrogen doping is able to facilitate the ORR via direct 4-electron transfer, thus with the highest efficiency. It is known that such catalytic activities can be altered even more, for example by functionalization of such nitrogen-doped graphene with electro-withdrawing surface groups, that would further modulate the charge and spin distribution on carbon active sites towards higher adsorption activities for oxygen. For the

most effective process, there is attempt to prepare N-doped graphene that would include only those N sites that accelerates the ORR the most. Type of nitrogen configuration in graphene network and its effect on catalytic properties is however still an issue of current research.

From most usual nitrogen configuration there is pyridinic N, graphitic N, pyrrolic N, amino group and pyridinic N. Each configuration has different nature, different abilities when incorporated into graphene lattice. Doped graphenes prepared by any synthetic approach commonly contain multi-configurations of nitrogen in final product. Current studies are focused to clarification of the type/types of nitrogen that is/are responsible for advanced catalytic abilities for ORR. Emphasis is put on the synthesis of single type of nitrogen in graphene, controlling the ratio of nitrogen types and evaluation of their respective contribution to ORR catalytic activity. Even though the clear results and explanations of each configuration are not established yet, the most promising candidates are pyridinic N and graphitic N.

Nitrogen doping procedure can be facilitated by either in-situ approach by laser ablation or chemical vapor deposition where doping occurs consistently with graphene synthesis, or via post-treatment approaches where doping is performed with existing graphene precursor. Advantages of post-treatment methods are large-scale production and inexpensive processing. Hydrothermal treatment is very advantageous post-treatment method for synthesis of heteroatom-doped graphenes with high and moldable volumes and high surface areas. In particular, such synthetic approach takes advantage of one-pot reduction of graphene oxide (GO) to reduced graphene oxide (rGO) with subsequent functionalization with nitrogen. Such method produces rGO-N hydrogels which after freeze-drying are converted into aerogels. This was proven by high utility of such materials for fabrication of sorption materials, capacitor materials, electrode substrates or electrochemical sensors[4,5,6].

In this work we were focused on preparation of N-doped graphenes via hydrothermal treatment that used graphene oxide (GO) as precursor. As nitrogen precursors we have chosen four different compounds: ethylenediamine, *p*-phenylenediamine, polyvinylpyrrolidone and ammonium hydroxide. Our aim was to control the hydrothermal synthesis conditions in order to study its influence onto the resulting type of nitrogen and ORR catalytic response. The ORR electro-catalytic properties have been characterized and compared in term of nitrogen type and content.

2. Fuel cells and oxygen reduction reaction

Today´s world automobile industry relies completely on fossil fuels despite the fact that fossil fuels (*i. e.* carbonaceous substances including mainly coal, oil or natural gas) are non-renewable and they have negative impact on the environment due to the huge production of CO_2, NO_x, SO_x and other greenhouse gases[7,8,9]. In fact, in European Union (EU), the greenhouse gas emissions from automotive industry increased by 23.1% between 1990 and 2015 and current automobile transport generates up to 72% of total greenhouse gas emissions, according to European Environmental Agency, 2017[10]. In America, in 2010 it was even more, up to 79%, according the Environmental Protection Agency[9]. For all above mentioned reasons, replacement of commonly used fossil fuels became highly urgent in all over the world. The new trend refers to the conversion of chemical energy to the electrical one, which can be realized via fuel cells. In this context, naturally friendly alternative fuel seems to be a hydrogen gas used in proton exchange membrane fuel cell (PEMFCs) that assume to be great candidate for cars in the future[1].

2.1. Principle of fuel cells

Fuel cell is an electrochemical cell that converts the chemical energy of a fuel into electrical energy through an electrochemical reaction[1]. The cell consists of two electrodes, *e. i.* cathode and anode as you can see in the Figure 1[11]. Anode and cathode are immersed into the electrolyte, separated from each other via semipermeable membrane and connected to external electric circuit. Each electrode is supplied with special substance – fuel is provided to the anode while oxidizing agent is given to the cathode.

The whole electrochemistry inside occurs on the electrode/electrolyte interface. Chemical reactions between fuel and oxidizing agent occur under applied voltage, where fuel is oxidized and oxidizing agent is reduced and thus an exchange of electric charges between these two substances arise. As a result, electrons flow simultaneously from negative (anode) to positive (cathode) electrode which generates electric current and portion of heat[3,12]. Fuel cells are different from batteries since in fuel cells the circuit is not closed. Therefore fuel cell cannot be discharged as battery and its reactions may happen all over again as long as the reactants are supplied. Since the oxidizing agent can be the air which is available everywhere, the only substance that need to be stored in stock is fuel.

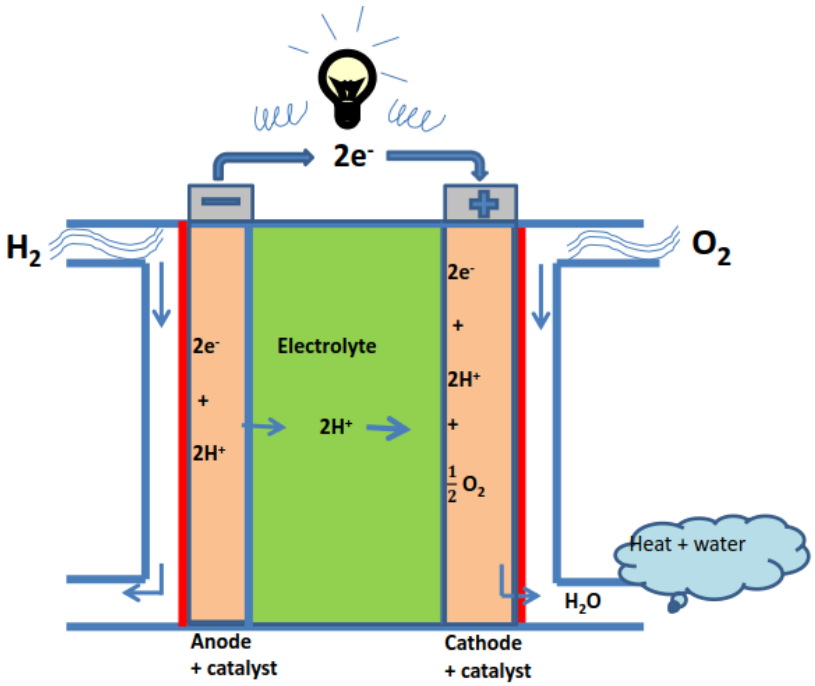

Figure 1. Scheme of proton exchange membrane fuel cell.

Type of fuel cells

Nowadays, there are several different types of fuel cells, typically classified by the kind of electrolyte they use and some of them reach back to 1960s[1]. Fuel cells suitable for stationary power generations include solid oxide fuel cell (SOFC), molten carbonate fuel cell (MFCS), and phosphoric acid fuel cell (PAFC). Transporting power generators need affordable working conditions like lower process temperature, lower noisiness. These requirements fulfill direct methanol fuel cell (DMCF), which uses methanol as the main fuel and aforementioned proton exchange membrane fuel cells (PEMFCs)[1] which use hydrogen as a fuel.

Nowadays, PEMFCs are most studied types of fuel cells[1,3,13] due to the world´s attempt to employ hydrogen as an environmentally friendly, renewable (by production from photochemical water splitting) and cost-effective fuel for transportation industry in near future (Energy Policy Act of 2005)[1]. PEMFC is specific type of electrochemical cell that consists of two electrodes (cathode and anode) covered with catalyst ink, immersed into electrolyte and separated from each other by gas diffusion layer. Chemical reaction occurring in PEMFCs uses hydrogen as a fuel and oxygen as oxidizing agent. By applying potential to the electrodes, liquid hydrogen is oxidized at the anode to H^+ cations which pass through the diffusion layer to the cathode and electrons which are transported to the cathode via external

circuit are used to reduce the molecular oxygen at the cathode. The passage of electrons via external circuit generates a large portion of electrical energy[1]. The incoming H^+ then react with O_2 and electrons together at the cathode surface and form water as the only chemical product.

Challenges and problems in fuel cell technology

The obstacle, which prevents the desire applicability become commercially available, is the cost of such fuel cells. The cost includes the fuel cell development and production as well as the infrastructure (gas stations) providing its utility for people. Another important fact is necessary investigation of hydrogen ecological production (green methods for hydrogen production) as well as the efficient hydrogen storage[14].

Last but not least, the overall cost also reflects the use of expensive catalyst, which is required for efficient energy conversion. Both hydrogen oxidation reaction (HOR) at the anode and oxygen reduction reaction (ORR) at the cathode requires catalysts. Study with the single platinum catalyst showed that the kinetics of hydrogen oxidation is fast and the needed amount of catalyst is negligible. On the other hand, the rate of ORR is about 5 orders of magnitude slower than in HOR[13]. For another illustration, catalysts formed by Pt nanoparticles using carbon black as support have 0.05 mg cm^{-2} loading on HOR and 0.4 mg cm^{-2} on ORR.

Therefore, current chemical research is focused especially to develop catalyst for the part of oxygen reduction[21]. This is an object of interest in latest research as well as in this thesis. Currently most efficient catalyst for both reactions is platinum (Pt), in the latest investigated form of electron-reduced Pt dispersed on carbon support (Pt/C) or core-shell Pt NPs[13].

2.2. Oxygen reduction reaction (ORR) and its mechanism

Reduction of oxygen happens daily in the life of biological cellular respiration when saccharides are degraded and in the presence of oxygen they produce energy in the form of ATP. In the context of fuel cells, the reduction of molecule of gas oxygen is a part of whole cell reaction when reduction of gas oxygen molecule is dependent on electrons produced by decomposition of gaseous hydrogen on the opposite electrode and only together they can react

continuously to produce portions of electrical energy. Unfortunately, unlike in biological systems, the ORR in fuel cells is not catalyzed automatically by enzymes.

In PEMFCs, the ORR takes place at the cathode and ORR in aqueous solutions occurs mainly by two pathways as you can see in Table 1[2]. There is direct 4-electron transfer from the electrode surface to the adsorbed oxygen molecule to form water and 2-electron transfer through H_2O_2 intermediate, resulting also in formation of water[2,13,15,16]. There is also 1-electron reduction pathway possible in non-aqueous aprotic medium; however, its utility is inefficient for fuel cell application and rather is used in investigation of ORR mechanism[2].

Several ORR studies highlight the direct 4-electron reduction as the most effective and desirable[2,13, 15,16]. Drawback of 2-electron pathway results in lower current densities, operating in low voltages or reducing the effective electron transfer number. Apart from that, forming of intermediate hydrogen peroxide (H_2O_2), as a strong oxidizing agent, brings a risk in degradation of the electrode membrane[13]. Nevertheless, in both cases, the kinetics of ORR is very slow and thus for practical applications in fuel cells, a cathode ORR catalyst is essential.

Two-electron transport pathways are usually seen on transition metal catalysts with lower activity (Hg or Au, Pt_3V or Pt_3Ti), whereas Pt catalyst is capable of direct 4-electron reduction[13,15,16]. Therefore, ORR catalysts are usually based on platinum (Pt). In the case of Pt, the rate of removing the adsorbed species from the electrode surface is limiting step, while in the case of weak bonding of Pt_3V or Au, the limiting factor of reaction rate is the slow transfer of electrons from the electrode surface to the adsorbed oxygen[16]. There is also an effect of the electrolyte on the thermodynamic electrode potentials (E^0) for ORR.

Table 1. ORR pathways in alkaline and acidic electrolyte. [Adapted from ref.[2]]

Electrolyte	ORR reactions
Acidic aqueous solution	$O_2 + 4H^+ + 4e^- \rightarrow H_2O$ $O_2 + 2H^+ + 2e^- \rightarrow H_2O_2$ $H_2O_2 + 2H^+ + 2e^- \rightarrow 2H_2O$
Alkaline aqueous solution	$O_2 + H_2O + 4e^- \rightarrow 4OH^-$ $O_2 + H_2O + 2e^- \rightarrow HO_2^- + OH^-$ $HO_2^- + H_2O + 2e^- \rightarrow 3OH^-$

The mechanism of ORR reaction is complex, involving multi-electron transfer processes composed on many elementary steps and involves many possible intermediates[13,15,16]. The essential part is O_2 breaking and theoretical calculations propose two options of its process. It can happen either at the moment as the oxygen molecule reaches the electrode surface (dissociative pathway) or after the oxygen molecule is adsorbed on it (associative pathway). The border between associative and dissociative mechanism probably lies at potential of 0.8 V, while at higher potential dominates the dissociative mechanism[17]. These suggestions were obtain using density functional theory (DFT) calculations of Pt[2,15,17].

In practice, every electrochemical reaction is set up by several processes where mass transport of reactants to the electrode surface (where the reaction of interest takes place) and charge transfers through the electrode-electrolyte interface are of most importance. These are processes of polarization and generally, there is activation, ohmic and concentration polarization presented on the electrode, which decreases the voltage of the fuel cell. The attempt of employing catalysts is to enhance the reaction rate. The ohmic polarization is intrinsic property of the cell[18] that cannot be deleted. On the other hand, concentration and activation polarization can be affected. Since the activation polarization is caused by the sluggish ORR kinetics, there is need of the good catalysts that can minimize the activation barrier for the reaction. For minimization on concentration polarization, the convection of solution has to be accurately controlled to obtain the current response completely unaffected.

For practical applications, the reaction variables include the properties of catalyst, electrolyte and the electrode surface[2]. Even though the investigations were studied on Pt based catalysts, their conclusions may be accepted as guiding lines helping to develop other classes of catalysts.

Techniques used in ORR

Techniques used for ORR electro-catalytic measurements and studying its mechanism and kinetics include usually cyclic voltammetry (CV), linear sweep voltammetry (LSV), measurements with rotating disc electrode (RDE) and/or rotating ring disc electrode (RRDE)[2]. As was mentioned before, to minimize concentration polarization, the convection of solution in controlled manner is preferable. In that case, the current response will be completely unaffected during measurement. While classical electrochemical methods like CV and LSV prefer quiescent solution for measurements, the RDE and RRDE methods (hydrodynamic

methods) prefer the active force that creates the convection on very controlled manner[19]. Principles of common ORR techniques are highlighted below.

Cyclic voltammetry is electro-analytical technique usually used as first method for basic electrochemical characterization of studied system. The most common set-up used for electroanalytical measurements consists of three electrodes including working electrode (WE), reference electrode (RE) and counter electrode (CE) connected to a potentiostat. In this case, the current flows between the CE and WE. The potential difference is controlled between the WE and the CE and measured between the RE and the WE. The potential between the WE and CE is not usually measured. The working electrode is the electrode at which the reaction of interest takes place and commonly is made of inert materials such as gold, platinum, silver, glassy carbon or mercury. The reference electrode possesses a stable and well-known electrode potential, thus it is used as a point of reference in the electrochemical cell as already mentioned. For this purpose, saturated calomel or silver/silver chloride electrodes are usually employed. The counter electrode (also known as auxiliary electrode), is an electrode which is used to close the current circuit in the electrochemical cell. Such electrodes are commonly made of platinum, graphite or other carbon material and usually it does not participate in the electrochemical reaction[12]. A potentiostat is employed to apply voltage into the electrochemical cell to induce redox reactions. Subsequently, generated Faradaic current is measured. As an output, cyclic voltammogram, depicted as current (I) vs. applied potential on the cell (E), is obtained (Figure 2). Despite voltage can be applied with different scan rates, it is always applied linearly with time dividing one cycle into forward scan (increasing of applied potential) and reverse scan (decreasing of applied potential). Oxidation and reduction peak heights (maximal anodic and cathodic currents) quantify the amount of analyte oxidized/reduced on the electrode surface, while the peaks position defines them qualitatively[20].

CV technique in analysis of ORR catalytic activity is used in order to observe whether the electrochemical process at the electrode surface is diffusion-controlled or not. We can also calculate the surface concentration of the catalysts from the slope of current (I) vs. scan rate (ν). More importantly, we can predict the catalytic activity from the position of onset potential and peak current of the voltammogram[2].

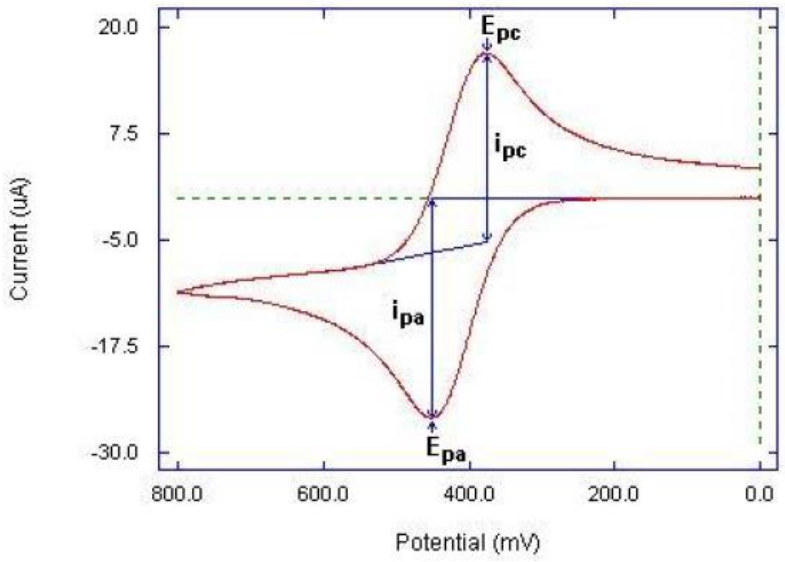

Figure 2. Illustration of cyclic voltammogram. Epc and Epa refers to peak potential of cathodic and anodic peak, respectively. Ipc and Ipa refers to cathodic and anodic peak current response, respectively. [Adapted from ref.[21]]

Linear sweep voltammetry (LSV) is the variation to CV technique; the experimental setup is realized in the same manner as mentioned above. However, as the name implies LSV consists only of forward scan (Figure 3). It is used to observe the process of oxidation or reduction of species presented in electrolyte so this technique is used usually for irreversible reactions (where reverse scan would bring no more information). By sweeping the potential between working and reference electrode the potential of working electrode shifts from its origin value (polarization) and thus initiates redox reaction. In the same manner as in CV, the difference between standard electrode potential (E^0) and potential of the reduction/oxidation observed experimentally is called over-potential ($\eta = E - E^0$). During the LSV measurement, the potential is increased linearly with time at fixed potential range and current response is recorded to obtain the LSV curve. Similarly as in case of CV, the peak potential clarifies the quality and the peak response determines the quantity of the analyte.

In the case of ORR, optimal results should depict the highest possible power density. This can be achieved by high current density recorded at high cell voltage[2]. The data for interpretation ORR performance includes Tafel slope and exchange current density which are obtained when plotting the over-potential vs. log current[2]. However, the steady-state experiments are prone to presence of solution convection by e.g. thermal gradient, which could easily disturb the collected current signal. Due to this limitation, a further establishment must be employed to force the solution to move in a controlled way, e.g. by ultrasonication or or rotation[19].

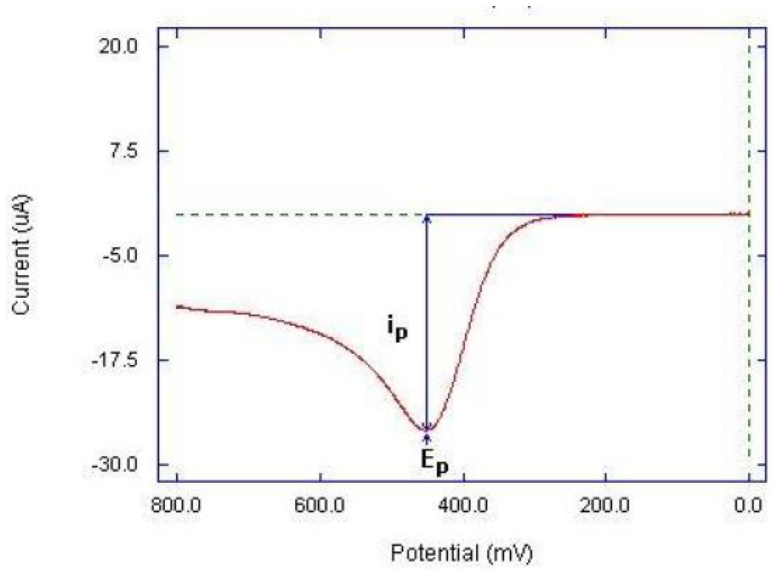

Figure 3. Illustration of linear sweep voltammogram. Here, Ep refers to peak potential of anodic peak, respectively. Ip refers to anodic peak current response. [Adapted from ref.[21]]

Rotating disc electrode (RDE) provides stable and steady-state laminar flow of the solution from the bulk to the electrode surface. This fact together with feasible construction, accurate measurements and sufficient theoretical background that correlates with experimental observations[22] makes the RDE one of the most used in ORR study and optimization of catalysis conditions. The invention of the first RDE electrode dates back to the early 1960´s, however, the theory describing the mass-transport controlling RDE was invented by Benjamin Levich in 1952[19]. RDE electrode is constructed of an electrode disc (usually Pt, glassy carbon or gold), which is embedded with an insulating material (usually Teflon or glass), into a rod shape[22,23] according to the Figure 4. This is connected to a motor which rotates the electrode in moldable frequencies according to desire rotation rates. This design of the electrode system takes advantage of developing the diffusion layer constant in time[23]. During the electrode rotation, the electrolyte flows from the bulk to the electrode surface, upwards perpendicularly to the surface (where the electrons from the electrode are added to the oxygen molecules) and by centrifugal force again back to the bulk solution. That is how the steady-state circulation of fresh electrolyte is achieved. There is a hydrodynamic boundary layer in the contact with the electrode surface in which the electrolyte rotates with the electrode. A thin layer of this area in very closest contact with the electrode surface is so called diffusion layer because within this layer the electrolyte reaches the electrode surface by only diffusion-controlled processes[19]. The overall mass transfer of the electrolyte is yet convective-diffusion controlled, following the theory of hydrodynamics[23]. When convection

of the solution is controlled, then the magnitude of the cathodic current is dependent only on the rate in which the oxidized solution is able to supply the electrode surface[19] having the maximum (saturated) value of the obtained current called the limiting current. This current is then mass-controlled. Therefore, we can increase the limiting current by increasing the concentration of electro-active species on the electrode surface, and this can be achieved by applying higher rotation rates[19].

Rotating ring disc electrode (RRDE) is an alternative to RDE which apart from disc electrode contains also second electrode, shaped into a ring that surround the working electrode – a ring electrode (Figure 4). This ring serves as a detector for those intermediates or even products with sufficiently long life time and so it is usually applied to study the chemical mechanisms of the electrochemical reactions. This innovation was suggested in 1958, six years after the describing the RDE[19]. Typically, when there is a reduction of electro-active species taking place at the disc electrode (applied required potential for reduction) then the products are back oxidized at the ring electrode (more positive potential applied). In this light, the ring electrode fulfills the performance of the reversible scans of the stationary electrodes[22]. Unstable intermediates decompose before they reach the ring electrode and therefore, the ring limiting current is usually smaller than disc limiting current. Based on the ratio between the ring and disc limiting currents (*i.e.*, collection efficiency of the RRDE), it is possible to predict the kinetics of the products and/or unstable intermediates. Generally, by applying higher rotation rates, the collection efficiency is getting closer to the empirical value obtained by measuring well-behaved redox system (*e. g* ferrocyanide/ferricyanide system). In the context of ORR, the RRDE electrodes are the most useful technique to elucidate different electron pathways[19].

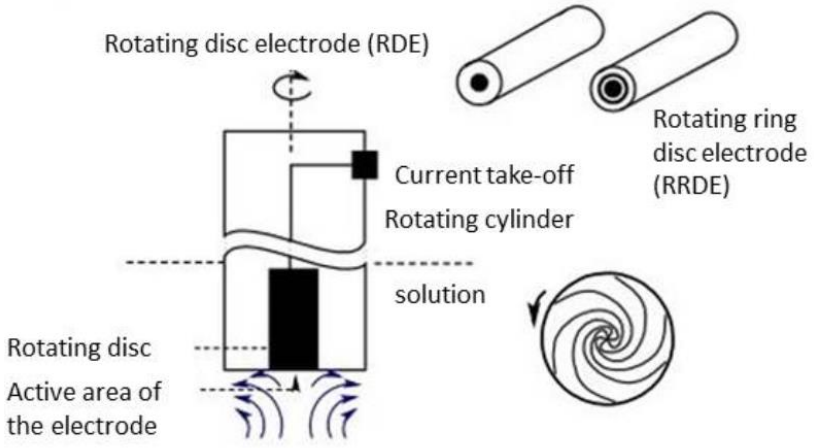

Figure 4. Scheme of rotating disc electrode and rotating ring disc electrode. [Adapted from ref.[24]]

3. Oxygen reduction reaction catalysts

In general, catalyst is a substance that facilitates the chemical reaction, especially its rate, at feasible conditions. The principal function is lowering the activation barrier for the reactants to be converted to products. The effectiveness, selectivity and uniqueness are related to catalyst unique structure and chemical properties. In the ideal case, catalyst does not interact either with the reactants or products and is ready for re-use after the reaction. In ORR, catalyst layer covers cathode surface. The used amount of catalyst reflects how much the reaction is slow and how efficient the catalytic activities of the catalyst are.

Requirements for ORR catalyst include activity, selectivity, stability and poisoning resistance. Selectivity of the catalyst to adsorption of oxygen is of most importance since it defines the pathway of oxygen reduction. Once again, when oxygen is adsorbed onto the catalyst surface without breaking (associative mechanism), hydrogen peroxide is formed, and therefore 2-electron inefficient mechanism is performed. In dissociative mechanism, oxygen double bond breaks upon adsorption onto the catalyst surface and thus direct 4-electron pathway is carried out.

Activity of ORR catalyst is evaluated by strength of oxygen binding. For optimal function, it is necessary to exhibit balanced absorption/desorption of reactant and product, respectively. If some of the process is too slow or too fast, it may slow down or even stop the reaction. Stability of catalyst includes also its ability to endure the operating conditions such as low or high pH, strong oxidants, reactive radicals or changes of temperature under applied voltage. Poisoning resistance means that work of catalyst is unaffected by impurities that are inevitable components of fuel cell operation and of feed gas, here hydrogen[25]. Also one has to take into account other phenomenon from which every PEM fuel cell suffers and that is hydrogen crossover. In order to supply more hydrogen ions to cathode and increases power density of the cell, very thin membranes are used in PEM cells. Since some portion of hydrogen gas is then able to penetrate through the membrane from anode to cathode side, it parasites on the cathode active sites, creates there mixed potential and degrades the membrane and whole fuel cell performance[26]. The tolerance of catalyst to this effect is therefore desirable.

3.1. Platinum catalysts

Nowadays, platinum-based materials are most common catalysts, used not only in ORR catalysis. Catalytic properties of platinum have been observed for the first time in hydrogen ignition in the early 1800s. Platinum is very unreactive element, non-corrosive at room temperature, insoluble in usual solvents and it has also great capacity for adsorption of hydrogen gas. Such precious character and mechanical stability makes platinum one of the best catalyst[27]. Particularly in ORR, platinum catalyst is the most comprehensively studied and most efficient as well. The layer of platinum that covers the cathode facilitates the adsorption of oxygen, the release of electrons and creates environment for their reaction with penetrated hydrogen ions.

The inevitable fact of platinum and every metal catalyst is that they undergo oxidation in oxygen presence. For platinum it means that at high potential such as ORR thermodynamical potential (1.23 V vs RHE), its surface properties change due to the simultaneous existence of pure Pt and PtO. The absorbed oxygen is thus bind strongly and is stable and unreactive. Only by lowering the potential, the electron transfer became possible and reduction of oxygen may proceed. This is explanation of over-potential of platinum catalyst in ORR[2,17].

ORR catalytic activity of platinum catalysts is highly structure-sensitive, which means that it is dependent on the crystallographic orientations of its surface[13]. Arrangement of surface atoms and surface/volume ratio affect the catalytic activity by characteristic adsorptions for oxygen or hydroxyl (OH). In general, high index planes of platinum such as (730), (210) and (520) with high densities of atomic steps, kinks and ledges possess higher catalytic activity than those with low index planes. From typical low index planes of surface of bulk platinum ((111), (100) and (110)), the most efficient in catalysis is (111). Nonetheless, such platinum nanocrystals have quite large particle size and their surface structure is unstable during the fuel cell performance. The stability is enabled by small platinum particles finely dispersed on porous support which enlarges the electrochemical active surface area and consequently catalytic activity[13]. Therefore, todays state-of-art commercially available Pt/C catalyst consist of porous carbon support loaded with dispersed platinum nanoparticles and covered with surface low index planes (100) and (111)[15]. Its efficiency is seen mainly in terms of the low over-potential and high current density.

Platinum catalyst is capable of dissociative mechanism. Platinum also exhibits highest activity among metal catalyst, which can be understood by ability to absorb the oxygen strongly enough to proceed the reaction but weakly enough to release products and renew the catalysts surface. This is depicted by highest activity as a function of oxygen binding energy from various tested metals. Stability of platinum under harsh fuel cell environment takes advantages of its highly precious character that prevents from dissolution, especially in acidic electrolytes. However, it is still a metal which tends to passivize it surface by oxidative layer which slow down the kinetics of ORR and subsequently hinders long-term stability of the fuel cell. The biggest drawback of platinum catalyst is suffering from sulfur impurities and carbon monoxide (CO) poisoning. This is exactly what points out on replacing pure platinum with platinum alloys which would increase the tolerance to this poisoning effect and thus hinder its degradability and increase the fuel cell capability in practical applications[25]. The driving force leading to replacing platinum catalysts are also high cost of platinum, nonrenewable sources of platinum and poor tolerance to hydrogen crossover effect.

Platinum-based catalyst

Firstly, research has re-directed from the pure Pt to the Pt-based catalysts, which could minimize the amount of Pt used, *e.g.* by loading small amount of Pt onto a conductive support or making alloys. In platinum alloys, the change of electronic structure like increasing of d-band vacancy and change of Pt-Pt distance subsequently changes the catalytic activity. The electrochemical activity varies then according to the type. Pure Pt catalysts possess highest stability, while Pt alloys possess highest activity. Core-shell Pt nanoparticles (NPs) catalysts have the middle performance. However, core-shell Pt NPs ranges among the most effective catalysts due to their balanced activity-stability relationship[13]. On the other hand, Pt catalysts have the minimal over-potential among all currently known catalyst for ORR.

Anyway, low stability under cell environment and environmental unfriendly sources still limit the practical application of Pt-based catalyst and therefore research dealing with new class of Pt-free catalysts has attracted huge interest.

3.2. Non-noble metal catalysts

Non-noble metal catalysts, such as quinones and its derivatives, transition metals and macrocyclic molecules, transition metal chalcogenides, metal carbides[2], nitrides and

phosphides[16] have been recently studied as possible catalysts for ORR. For illustration, there were composites of mainly Co-Fe together with carbon support in addition to nitrogen or conductive polymer[16]. Worth mentioning are nickel based metal-organic frameworks (MOFs) mixed with nitrogen doped graphene oxide composite as efficient electro-catalysts[28] or glassy carbon-supported Mn_3O_4 composite with long-term stability[15]. However, the latest trend is mainly focusing on metal-free catalysts, which could fulfill even the ecological point of view.

3.3. Metal-free catalysts

Among other group of catalysts, such as metal-organic frameworks and covalent-organic materials, metal-free carbon materials especially those based on graphene are considered to be very promising. Such materials include graphite, carbon nanotubes, ordered mesoporous carbon. They are all used as support material for tuning its properties by heteroatom doping. There are binary or trinary-doped carbon-based materials, nitrogen-doped ordered mesoporous arrays with silica template *etc*[15]. Graphene-based materials were proved to have excellent predispositions for energy storage applications, batteries, supercapacitors and energy conversion devices[29,30,31]. Moreover, such materials are easily moldable to various volumes and offer the possibility to tune the electronic properties by heteroatom doping. Such properties are crucial for ORR catalysts. In the case of heteroatom doping, nitrogen, boron, phosphor or sulfur[32] are commonly used to upgrade electronic properties of considered material.

3.3.1. Graphene-based catalysts frameworks

Graphene

Graphene, as 2D crystalline form of carbon can be imagined as a repetition of carbon atoms shaped into a hexagon which, when extended in plane, form honeycomb-like carbon network. Such single layer is only a carbon atom in height (0.34 nm) and corresponds to the sp^2 carbon hybridization[33]. Unlike it seems that thermal fluctuations may easily disrupt the plane of such small thickness and possession of very low melting point would create the instability[34,35], in fact, graphene is capable to hinder these effects and minimize the free energy due to its perfectly designed wrinkled structure, strong in-plane atoms bonding and minimal height[33,36]. Every carbon atom has 4 valence electrons, 3 of them are used to form in-plane σ bond with other 3 carbons and the 4^{th} one is situated perpendicularly to the network

forming valence and conductive bends above and below the aromatic plane. In this situation the electrons and holes are actually meeting at certain points - just where Fermi level lies. As a consequence of π-π conjugation along the plane, there is a strong anisotropy which facilitates all the electrons and charges to propagate through the strong in-plane π-π interactions rather than along the perpendicularly formed weak Van der Waals forces[33]. In theoretical model of monolayer graphene, the electrons move along the plane with no resistivity, very fast, the material behaves like semiconductor and possesses many unique merits such as thermal conductivity, large charge mobility and huge mechanical resistance. Each of these properties is highly dependent on the number of layers in graphene, especially the electronic properties. It can be clearly seen on the example of monolayer graphene acting like semiconductor and bulk layered graphite act as semi-metal[33,35,37].

Even though theoretical properties of graphene are tremendous and promise advancement use in nano-opto-electronics, electrochemical applications or supercapacitors, in fact, pristine graphene sheets tend to stack together which changes significantly its overall properties and its direct utility is disallowed. For practical applicability of graphene, it is crucial to convert it into dispersible and stable intermediate in various solvents which would proceed further reactions, functionalization, but foremost to stay protected from stacking and agglomeration[38].

Graphene oxide (GO)

Nowadays, functionalization of graphene is necessary step for its practical usage and oxidation of graphene to graphene oxide (GO) was established as the most optimal option. It was declared as very ideal starting material for preparation of various graphene-based structures. In GO, graphene network is covered with reactive sites - oxygen containing functional groups such as hydroxyl-, carboxyl-, epoxy- and carbonyl-. These groups are mainly localized at the edges of the GO sheets[39,40]. GO´s unique merits result from repulsive forces between neighboring oxygen rich functionalities and the overall negatively charged surface protects the solution stability due to negative values of zeta potential which are below -30 mV in majority of pH range[41]. Oxygen content is required also for successful functionalization with additional molecules and/or atoms during various types of interactions, covalent or non-covalent. The higher is the oxygen content, the higher loading of an additive might be achieved[42]. Due to its easy solubility in water and its stability it facilitates large scale production and production of variety of modified graphene structures.

Preparation of GO has been updated since its first synthesis in 1859, a long before single graphene was discovered. Various ways of synthesis are summarized in Table 2. The most common preparation method is Hummers method whose mechanism is depicted Figure 5.

Table 2. Summary of development of the graphene oxide preparation.

Year	Author	Reagents	
1859	Brodie	Graphite flakes	fuming HNO_3 + $KClO_3$
1898	Staudenmaier		fuming HNO_3 + conc.H_2SO_4 + $KClO_3$
1937	Hofmann		conc. HNO_3 + conc.H_2SO_4 + $KClO_3$
1958	Hummers		conc.H_2SO_4 + $NaNO_3$ + $KMnO_4$

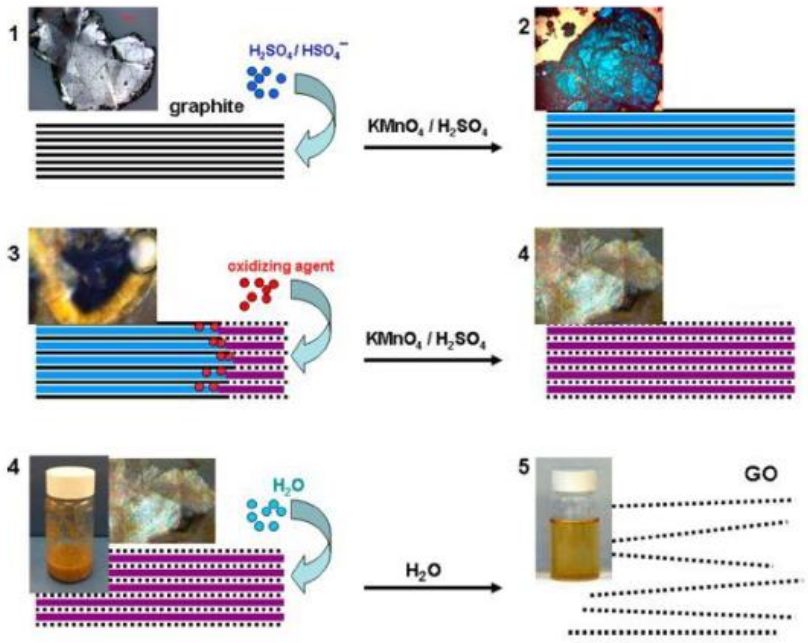

Figure 5. Schematic mechanism of the Hummers synthetic method for graphene oxide preparation [Adapted from ref.[43]].

Even the oxygen groups are essential for water dispersibility and participation in chemical reactions[43], they cause serious decrease in electrical conductivity of GO[4,41]. This is why GO needs to be partially reduced to rGO when it is desired to be applied in electrochemical or electronic applications[41,44].

Reduced graphene oxide structures (rGO)

Optimal conditions have to be respected to increase the conductivity while retain the anti-stacking and reactive behavior of rGO. Reduction of GO may be achieved via various approaches, such as thermal reduction or pyrolysis, chemical reduction (with hydrazine monohydrate) or electrochemically[12]. Because these methods are unable to reduce oxygen functionalities completely, their residues still act as active sites for further reactions and processing. As meaningful reduction option for ORR purposes, there is also possibility to convert rGO into spongy, foam-like, 3D hydrogel or aerogel architecture via hydrothermal reduction and freeze-drying. Other possibilities are also cross-linking and polymerization reactions[45]. The crucial role in these processes is creation of high surface area. Such structures obtained much interest among scientists due to its low density, high moldable volume, big surface area and efficient multidimensional pathways for electron transfers[30,31,46].

Before we take a deep insight into these hybrid nanomaterials, let´s point out the fact that such materials have a significant level of defects in their structure. These defects are assumed as the centers where the π-π conjugation disrupts[47]. Many reports showed that defects in graphene might play role in the ORR catalytic activity[47,48] in terms of onset potential improvement as well as current densities compared to pristine graphene planes[48].

4. Nitrogen-doped graphene-based structures

Latest research of heteroatom doping of graphene-based materials focuses mainly on nitrogen doping. It is undoubtedly one of the most studied approaches for functionalization of graphene towards electro-active material. Such materials showed great potential not only for ORR but also in construction of biocatalyst for hydrogen evolution reaction (HER) and oxygen evolution reaction (OER) in solar watter-splitting[28], as well as in electro-sensing of biological important substances[49] or creation of aptasensors for bacteria detection[50].

Nitrogen content has a positive effect on specific capacitance[51] and generally on overall electro-analytical performance. Creation of unique properties lies in modulation of the band gap, electronegativity and contribution to the aromatic conjugation. The impact to the electro-catalytic activity in ORR and its origin is, however, still not that clear and one can found controversy in the literature.

In following section there will be described theoretical as well as experimentally observed properties of N-doped graphenes and potential ways of their synthesis, since controlled synthesis of N-doped graphenes towards ORR activities was aim of this work.

4.1. Properties

Nitrogen atom has similar size as C atom; it possesses a free electron pair due to its five valence electrons and usually trivalent bonding. This makes it more electronegative in graphene network and introducing charge distribution and spin density modifications[52]. Changed charge distribution of carbon atoms leads to formation of active sites that participate in ORR as it will be discussed later[52].

In general, nitrogen can be incorporate into the graphene network by 5 main species: as graphitic N, pyridinic N, pyrrolic N, amino groups or N oxides. Pyridinic N bonds usually with two adjacent C atoms at the edges or in defect site. Graphitic N directly substitutes one C atoms in the graphitic network and pyrrolic N bonds also to two adjacent C atoms, but into only 5 membered ring and is as the only one in the sp^3 hybridization. Nitrogen oxides are formed on pyridinic N (N^+-O^-), located presumably at the edges. Amino groups are attached with σ bonds to any C atom, usually at the edges. Whereas pyridinic N contributes with one electron to the conjugation with aromatic system, graphitic N contributes with its two π electrons[53].

While nitrogen is incorporated within GO structure, the free electron pair conjugates with aromatic network[38]. The quantum behavior of the graphene lattice changes significantly. Very similar in-plane bond length of C-N to that of C-C does not disrupt the planar graphene structure. On the other hand, the inter-layer asymmetry originated from N-doping leads to opening the zero band gap and reaching the value about 0.14 eV (for single atom doping)[54,55] which creates n-type semiconducting behavior when compared to pristine graphene. The possibility to modulate the conductivity via adjusting the band gap (e.g. by increasing nitrogen loading) brings enhancement in power capability, power density and cycle life in battery and transistor industry[31]. More importantly, nitrogen induces charge/discharge rate much faster and specific capacitance much higher in addition to stability of the material when incorporated into the graphene network[56]. As a consequence, the electrical conductivity is much increased[57,58] as well as the overall electrical properties. In addition, microporous

structure can be tuned by adjustable amount of nitrogen precursor used in the synthesis. This is advantageous in fields like electrochemical sensing or supercapacitors[30,31].

To date, several N-doped graphene structures were synthetized with advanced properties towards ORR. Zhang *et al.* prepared N-doped carbon aerogels with pyridinic, pyrrolic and quaternary N, showing high specific capacitance, high catalytic activities towards ORR, methanol tolerance and high durability[59]. Pyrrolic and pyridinic N in 3D graphene framework presented by Zhao *et al.*, also showed direct-4 electron pathway for ORR with high diffusion current density[46]. Pyridinic, pyrrolic, quaternary, oxidized and chemisorbed N were doped onto single-walled carbon nanotube and exhibited efficient performance for ORR and also OER[60].

Such nitrogen configurations varies in term of both structure and electro-chemical properties. To date, the 100% sure result of which type of nitrogen configuration is most responsible for the ORR catalytic activity remains ambiguous. Numerous of theoretical studies as well as experimental tests that were carried out claiming opposite results, with pyridinic N[61] and graphitic N[62] being the most cited as responsible for active sites origin. However, also pyrrolic N[63] was proved to have some effect. There is great interest to multiple the active sites in N-doped graphene catalysts to the maximum. Therefore, it is urgent to produce just one nitrogen type and to clear understand its contribution to electro-catalytic activity. However, to synthetize the specific N configuration or their controllable ratio is very challenging and many variables contribute to the synthesis. Among possibilities, *e.g.* type of nitrogen precursor seems to be one way how to influence the nitrogen composition, as will be discussed later in the text.

4.2. Synthesis

There are several pathways for N-doped graphene synthesis, as well as there are various nitrogen precursors that can be used. For illustration, common nitrogen sources are urea, ammonia, melamine or pyrrole which were employed for synthesis graphene based materials showing the enhanced conductivity, charge mobility, stability[64,65] as well as enhanced catalytic activity towards ORR[66]. For curiosity, apart from the traditional methods, there was used for example pomelo peel as C and N source at once for synthesis of catalyst used for H_2O_2 production[67]. In fact, significant attempt is focused on utility of non-toxic and non-

aggressive compounds, which lacks in usually used small N molecules like pyridine, pyrrole, melamine, aniline or ammonia[59].

Material properties highly depend on the synthetic route, on the doping conditions as well as on the type and properties of graphene/carbon precursor[42]. Desired is to produce material with appropriate N type and quality. Generally, there are two basic synthetic approaches – in situ methods and post-treatment methods.

In-situ methods of syntheses

In situ approaches including laser ablation, chemical vapor deposition (CVD) or arc-discharge method. During these syntheses, process of N doping is done during the growth of the graphene/carbon substrate. Such process requires very precise conditions and expensive equipment. Even though the products are of high quality, the yield is low[42].

Panchakarla *et al.*[68] presented unconventional **arc discharge synthetic method**, based on molecular charge transfer. It is performed in arc chamber with two graphite electrodes filled with ammonia or pyridine vapors in hydrogen or helium carrying gases. Applied direct current arc voltage causes discharge of the gas-mixture and N-doped soot is deposited inside the chamber[36].

Laser ablation method uses laser pulses to ablate the pre-baked graphite target under the carrying gas – nitrogen, at very high temperatures reaching up to 1100 °C. The graphite is commonly rotated to perform uniform ablation. This technique is usually applied for synthesis of N-doped fullerenes and this method allows high control over the synthesis by controlling the laser operation[69].

Technique based on **chemical vapor deposition (CVD)** needs a substrate onto which, under very high temperatures ranging between 800 to 1000 °C, the mixture of carrying C-containing and N-containing gas are deposited. The substrates are most commonly Cu or SiO_2/Si or Cu/Si coated with Ni[36]. As carrying gas there is usually methane or ethylene/hydrogen mixture and ammonia gas is commonly used as N source. The flow rate can be modulated to control the N:C ratio presented in the final material, which possesses high crystallite structure[66]. However, the type of N configuration cannot be affected by change of time nor temperature of the synthesis process[70].

Post-treatment methods of syntheses

Post-treatment includes such processes that functionalize existing graphene/carbon precursors with various kinds of nitrogen source resulting in high nitrogen content. Such synthetic methods take advantage of cost-effectiveness and large scale production. Typical examples are thermal annealing or hydrothermaltreatment[42].

In case of **thermal annealing** (also pyrolysis), the precursors of graphene and nitrogen are mixed and placed into quartz tube into a furnace to undergo thermal reactions under inert atmosphere (N_2, Ar), during which the temperature increases slowly and ranges from 300 °C up to 1000 °C. Example of nitrogen precursor for this treatment can be melamine[49] or N-containing polymers[52], commonly used carbon precursor is GO[62]. The precursors may be used either both in solid state or firstly mixed in a solution and dried as a composite before pyrolysis. Big advantage of this method is quite explored system of controlling the nitrogen configuration only by changing the temperature. Generally, in annealing temperatures up to 500 °C the doping realizes especially on the edge and defect sites, while the higher temperatures nitrogen dopant are able to penetrate into the basal plane of the graphene network. The transformation of nitrogen configuration depending on the temperature is following: with rising temperature from 200 °C to 700 °C the pyrrolic N is transformed to pyridinic and then to graphitic N, respectively[71]. Controlling of the resulting structure is nearly impossible at higher annealing temperatures, in addition to evolution of toxic gases. On the other hand, higher temperature brings advantage of higher expansions of the reaction mixture as a consequence of high pressure initiation[72]. One disadvantage is hidden in the shift of 4-electron reduction to 2-electron reduction pathway with increasing annealing temperature, even though it enables to reach higher limiting current density[70] of such materials.

Hydrothermal treatment is advantageous option for synthesis of N-doped graphene structures for its facile, mild, large-scale, very effective and low-cost nature[36,38,51,73,]. Typically, the treatment consists of mixing GO precursor with nitrogen precursor under the elevated temperature, mostly at 180 °C[30,31,46]. As nitrogen precursor, any N-containing molecule can be used, like urea, ammonia, melamine, amines and any others. Synthesis facilitates one-pot reduction of GO to rGO and functionalization of rGO with nitrogen[29,65]. Unlike the strong reducing agents (*e.g.* hydrazine) in chemical reduction method, thermal reduction expresses more sites for doping[74]. In contrast to pyrolysis method, mild wet process

takes advantage of energy less consuming processing. It is facile yet effective approach for reduction of surface oxygen and restoration of electrical conductivity. Conductivity is even altered by nitrogen incorporation. In this method, GO self-assemble into rGO 3D hydrogel due to delocalized and random distribution of oxygen functionalities on GO.

Hydrogel structures bring advantages in many application fields owing to its special volume adjusting. Inside the hydrogels, cross-linking can be represented by long chain nitrogen molecule stitching rGO sheets which can then supply enough movement space for rGO sheets when loading and absorbing energy. This feature applies in supercapacitors, but even in fuel cell catalysis. It is possible to control the volume of the hydrogel by the amount of the N-source proportionally, in some cases also by the type of nitrogen molecule[31,73]. Moreover, when hydrothermal treatment is followed by freeze-drying, rGO hydrogels (GH) are converted into aerogels (GA). Schematic reaction process is illustrated in Figure 6.

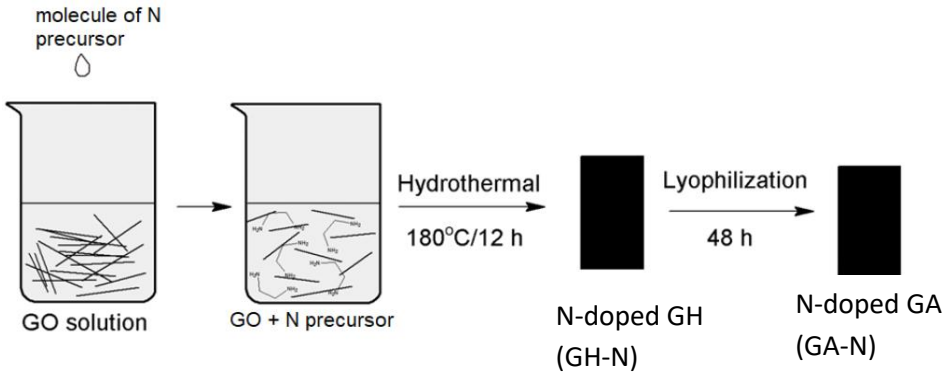

Figure 6. Scheme of hydrothermal preparation of GA-N followed by freeze-drying.

Aerogels represent the class of materials paving its applicability since 1930´s when they were prepared for the first time. Since then, they are attracting applications such as sorption materials[73], electrode substrates[4,75], catalytic supports, advanced electrochemical sensors[6] and energy storages especially when they are conductive[59]. GA-based structures doped with nitrogen then links two main properties – aerogel high volume composition with advanced conductivity due to renewed graphitic network enriched by conductive dopant. For imagination, the benefit may be seen in attracting positive ions of electrolyte due to its negativity and buffering their high volumes, thus increasing the specific capacity. Then, as a consequence of original defects and vacancies in the graphene lattice and those introduced with the doping process, pathways for positive ions transfer are created throughout the lattice. Even those big in diameter (e.g. Li^+) might diffuse into the structure. This is crucial in applications such as batteries, where high energy density and electrochemical performance

needs fast diffusion of ions at the first place[76]. Another pivotal application is in catalysis, energy storage devices and field of adsorption and/or capacitor construction[29,31,46,77].

There is also discussion in the literature which GO synthetic route is most favorable for following nitrogen doping procedure. The latest statement reveals that Hummers method exhibited advantages in the highest possible nitrogen loading, especially highest pyridinic N loading and the highest surface area of the prepared samples[78].

Owing to its cost-quality-scale-up ratio, chemical vapor deposition (CVD), thermal annealing and some percentage of hydrothermal approach, are the most preferable techniques for synthesis of N-doped carbon base catalysts for ORR application.

4.3. ORR catalytic activity on N-doped graphene aerogels

In order to prepare an ideal N-doped graphene catalyst, there are a lot of variables that need to be matched in a specific combination and conditions, among which high surface area, charge and spin distribution along the graphene network and type of nitrogen configuration is of great importance.

Catalytic activity of the N-doped graphene catalyst depends on the type of nitrogen configuration rather than on nitrogen content and higher importance over overall nitrogen content in the catalyst material gains high surface area (HAS)[29,52,74,79,80,81]. Porosity and 3D architecture of the catalyst are key factors for facilitating the excellent oxygen diffusion within the catalyst, leading to higher activity. 3D structure is beneficial for N-doped graphene-based catalysts made from GO, because in such structures there is avoided the re-stacking of the graphene sheets[82]. Even though the N-doped graphene catalyst with porous morphology performed higher over-potential than commercial Pt/C catalyst, in some cases they were able to increase diffusion current density instead[46]. For illustration, it was shown that the type and amount of particular nitrogen precursor has considerable influence on the final electrochemical properties, especially supercapacitor performance[31]. From this point of view, the content of nitrogen dopant should be controlled.

Nowadays, investigations are however focused on the question which type of nitrogen configuration is responsible (if there are more, then which the most) for the ORR catalysis and what kind of mechanism such activity facilitates. There are many researches trying to produce N-doped graphene-based catalysts with controllable type of nitrogen dopant in the

final material. From numerous studies, there were highlighted three main candidates performing the catalytic activity; they are pyridinic N, graphitic N and pyrrolic N, as shown in the Figure 7.

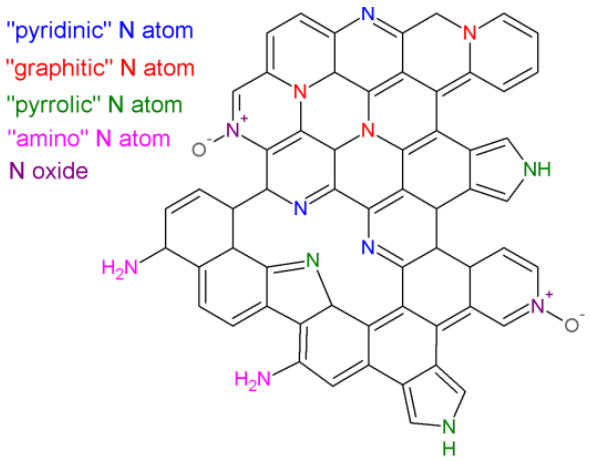

Figure 7. Scheme of nitrogen configurations incorporated into graphene lattice after functionalization.

It is known that all three configurations are useful somehow under some environment. The role of each of the three nitrogen types was found by various research groups[45,80]. Graphitic N was found to decrease intrinsic resistance and thus is was responsible for increment of electrical conductivity and transport of electrons to the electrode surface and also increased limiting current density of the catalyst material. Pyridinic N improved the onset potential of the ORR and shifted the mechanism towards direct 4-electron pathway[70]. Pyrrolic N participated in the weak H-bond formation and pyridinic N created intra-molecular H bonds as well. Both pyridinic and pyrrolic N were assumed to contribute to the pseudo-capacitance of the prepared material. Altered specific capacitance of the material was assumed to arise from N content and 3D structure which hindered the agglomeration[59].

Theoretical calculation performed by Guo *et al.*[61] suggested that the free electron pair of pyridinic N may be donated to the π- π conjugation and thus created Lewis basicity to the sample. Actually, C atoms situated next to the pyridinic N dopants could act as Lewis bases and therefore were marked as active sites for oxygen molecule adsorption. As a consequence of the reaction between the active C atom and OH group the pyridinic configuration changes to pyridonic configuration, as may be seen in the Figure 8. Note that these studies were performed in acidic media.

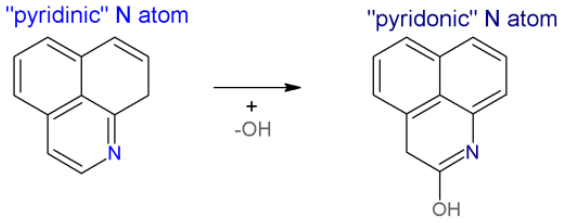

Figure 8. Schematic transformation of pyridinic N to pyridonic N as a consequence of reaction between carbon atom adjacent to pyridinic N and OH group.

From the side preferring graphitic N, there was shown lower energetic barrier for the oxygen dissociation on the graphitic N than on pyridinic N. Thus, even though both pyridinic and graphitic N withdrawn electrons from adjacent C atoms and create them positive, they differ in catalytic activities due to their distinct inner electronic character[62]. Higher potential for oxygen adsorption on graphitic N, due to higher adsorption energy was confirmed by others[77]. Different opinions were published on the role of pyridinic[70,83] and/or graphitic[84] N. Graphitic N was determined as more stable in contrast to pyridinic N, although they are believed to promote the ORR activity together[85]. Indeed, recent study showed that increased ORR catalytic activity was caused by presence of different N dopants[77].

Pyrrolic N was found to be active for supercapacitor applications where it increased supercapacitance of electric double layer capacitors. According to DFT calculation it was caused by the fact that it most suitably bind the electrolyte ions[63].

In general, controlling of the nitrogen configuration in catalyst material might be possible by the choice of nitrogen precursor, synthetic method and the temperature of the particular synthetic method used, especially during annealing preparation[62]. Pure graphitic N was prepared by CVD preparation method using julolidine as precursor[86] or by ethylene and hydrogen gas deposition in the presence of ammonia[83]. Purely pyridinic N-doped graphene catalyst was achieved by the same CVD method using pyridine gas as N source. Similarity between the chemical composition of nitrogen precursor (*i.e.*, pyridine, julolidine) and the nitrogen configuration of graphitic network structure could be possible condition for controlled synthesis, like was shown in study above[86] (Figure 9).

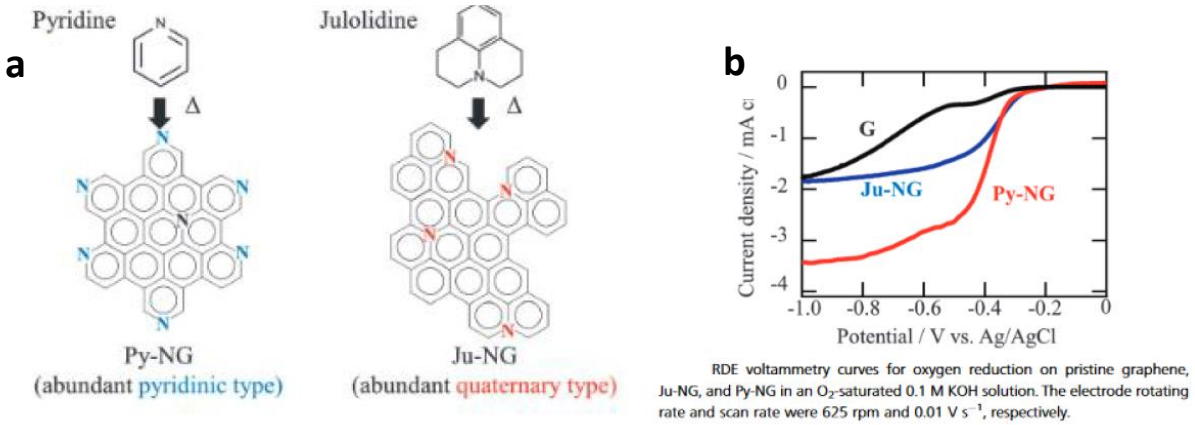

Figure 9. a) Schematic image of selective nitrogen doping into graphene lattice using aromatic molecules. b) LSV curve for ORR catalysis in O_2-saturated 0.1M KOH for pristine graphene, juolidone-doped graphene (Ju-NG) and pyridine-doped graphene (Py-NG). [Adapted from ref.[86]]

Other direction dealing with catalyst properties focuses on the inner structure of the catalyst. Pyridinic and pyrrolic type of nitrogen linked the relation of catalytic activity to the electron spin density and atomic charge density distributions[62,66,87,88]. Nitrogen dopant with withdrawing properties creates net positive charge in the neighboring C atoms to be ready to collect electrons from anode and use them for reduction of oxygen molecules[59]. Such activation of C atoms is caused by conjugating of its π electrons with lone electron pair of nitrogen as a consequence of disrupted conjugation of aromatic network[47]. Therefore, highly desire is to bring local asymmetry into the graphene charge and spin density distribution by any kind of nitrogen dopant, either substituted into the graphene lattice or attached to the plane perpendicularly. According to the literature, spin density is regarded as agent affecting the position selectivity for adsorption and charge density is responsible for attractive forces with charged atoms[85,89,90].

Another study[90] also indicated that nitrogen precursor with additional electron withdrawing substituents exhibited higher activity towards ORR because they effectively polarize the αC-N bond. This polarization is caused by higher electronegativity difference introduced by highly electronegative substituent to the catalyst. As a consequence of higher polarization for ORR the adsorption energy for oxygen decreases and the direct 4-electron reduction was prioritized.

In this thesis, we focused to the hydrothermal treatment to produce N-doped graphene structures with different kinds of N configuration inside, find the way how to control their content and confront it with their ORR activity.

5. Experiments

Materials

All chemical reagents used in this work were of analytical grade used as received without further purification.

5.1. Synthesis of materials

Graphene oxide

The process of fabrication followed the Hummer´s method, consisting of oxidation of graphite in acidic environment[91]. In a typical procedure, graphite flakes (2 g, 1 wt% eqv.) were mixed with $NaNO_3$ (1 g, 0.5 wt% eqv.) and concentrated H_2SO_4 (46 mL) was then added to this mixture. Consequently, $KMnO_4$ (6 g, 3 wt% equiv.) was dropwised resulted in exothermic reaction. For this reason, ice bath was used in order to keep the temperature below 20 °C during $KMnO_4$ addition. Afterwards, the reaction mixture was heated to 35 °C using oil bath and let stirred for 30 min. Then, DI water (92 mL) was added in small portions to keep the temperature at 98 °C and this temperature was maintained for another 15 min. After short cooling in water bath, DI water (200 mL) and 30% H_2O_2 (2 mL) were added into the reaction mixture, producing the last exothermic reaction. The reaction mixture was air cooled and stirred overnight.

Then, the as prepared mixture was collected by centrifugation. Final purification started with addition of HCl (2 mL) to dissolve the metallic residues inherited from $KMnO_4$. Afterwards, mixure was thoroughly washed by DI water using centrifugation in order to neutralize the acidic environment arised from H_2SO_4. Furthermore, ethanol was used for washing to the neutral pH and obtained material was vacuum dried at 70 °C overnight. As prepared GO solid phase (3.37 g) was removed from the oven and after air cooling was grinded to obtain a fine powder for further reaction.

Nitrogen doped graphene hydrogels and aerogels

Initially, un-doped graphene hydrogel (GH) was prepared from GO by hydrothermal reaction with subsequent freeze-drying process to produce porous aerogel (GA). Typically, GO (34 mg) was dispersed in DI water (17 mL) and exposed to ultrasound for 45 min, with

temperature reaching up to maximal 55 °C, in order to obtain black homogeneous dispersion. As final step, the GO dispersion was transferred into a Teflon autoclave, and placed into an oven at 180 °C for 12 h. By hydrothermal treatment, GO was reduced to hydrogel form. Obtained product was afterward washed with water to neutral pH and then was immersed in liquid nitrogen and freeze-dried overnight leaving behind GA aerogel.

Synthesis of nitrogen-doped GA was carried out by same hydrothermal procedure mentioned above where different nitrogen precursor (*i.e.,* ethylenediamine, p-phenylenediamine, polyvinylpyrrolidone and ammonium hydroxide) were added into GO dispersion. Detailed syntheses are described below.

GA-N(EDA)

In this case, ethylenediamine (EDA)[31] was used as nitrogen precursor in order to obtain N-doped GA aerogel following previously mentioned procedure. Additionally, three different ratios between GO and EDA was used for such synthesis progressively 12.2 μL, 37.7 μL or 100 μL of EDA was added to GO dispersion. After hydrothermal treatment and subsequent freeze-drying 3 differed samples with high porous-like structure and volume density were obtained and labeled in following way – GA-N(EDA 3:1), GA-N(EDA 1:1) and GA-N(EDA 1:3), respectively.

Sample labeled as GA-N (EDA 1:1) was also prepared by hydrothermal treatment with reduced time: original 12h was shorted to 3h. This sample was referred as GA-N (EDA 1:1)3h.

GA-N(PVP)

Typically, GO (20 mg) was dispersed in DI water (20 mL) and exposed to ultrasound for 45 min, with temperature reaching up to maximal 55 °C, to obtain black homogeneous dispersion. After that, poly(vinyl)pyrrolidone (PVP,2 mg)[82] was added and stirred for 30 min. After fine dispersion was obtained, 15 mL of dispersion was mixed with ascorbic acid (0.75 mL) and stirred again for 30 min. Finally, this mixture was transferred into a Teflon autoclave, and placed into an oven at 180 °C for 12 h. The same washing and freeze-drying procedure as in the case of un-doped GA was then applied.

GA-N(pPDA)

Typically, GO (30 mg) was dispersed in DI water (15 mL) and exposed to ultrasound for 45 min, with temperature reaching up to maximal 55 °C, to obtain black homogeneous dispersion. After that, *p*-phenylenediamine (pPDA, 4 mg)[29] dispersed in 2 mL of ethanol was added, and 10 min ultrasonication was performed; followed by same hydrothermal, washing and freeze-drying procedure as described previously for un-doped GA.

GA-N(NH_4OH)

Typically, GO (50 mg) was dispersed in DI water (25 mL) and exposed to ultrasound for 2 h, with temperature reaching to 55 °C, to obtain clear dispersion. After that, EDA (530 μL) and NH_4OH (130 μL)[92] were added. The reaction mixture was placed into water bath, heated to 95 °C and maintained with constant stirring for 5 h. As final step, the obtained hydrogel was immersed in liquid nitrogen and freeze-dried overnight as described previously for un-doped GA.

5.2. Characterization techniques

All samples were examined and characterized by following microscopic and spectroscopic techniques. Short introductions to their principles are given in following text.

Electron microscopy allows much higher resolution and magnification of the obtained images compared to optical one. Such images are facilitated by beam of electrons with ultra-small wavelength deposited on material, which allow theoretical resolution up to 0.1 nm. Electron microscopes use electron guns that generate electron beam, they use special electromagnetic lenses and vacuum equipped instrumentation. The high resolution is achieved by acceleration voltage. The higher acceleration voltage, the higher electron energy, the lower electron wavelength and the higher microscope resolution[93].

While taking into account scanning electron microscopy (SEM), scanning/raster over sample surface by focused beam of electrons is performed. The brightness of the beam is necessary for very high imaging quality. As a result of applied electron beam, electrons are emitted/scattered from the specimen. The signal electrons that are emitted from specimen are detected and image is formed on a display screen. Scattered electrons may result from scattering of incident electrons on the atom of specimen or from ejecting electrons from atom

in the specimen. While the former gives information about elemental composition, the latter generate topographic contrast.

Other technique known as transmission electron microscopy (TEM) uses illumination of specimen to form the images. Electron gun produces electrons that are accelerated and condensate on the specimen. The accelerated voltage is much higher than in SEM technique. Sample must be able to transmit electrons, which after passing through specimen are deposited onto fluorescent screen or photographic film or CCD[93].

Fourier transform infra-red spectroscopy (FTIR) determines molecule structure on the bases of interaction of nuclear vibration in molecules with electromagnetic irradiation. In this method infra-red radiation is focused and passes through the specimen, which as a response changes its dipole moment and also rotational-vibrational state. Radiation energy changes according to the interference with the vibration of the molecules and generated vibration signals (characteristic for each bond) are detected on thermal/electric detector. The detector converts the light signal to the electric signals. Detectors including Fourier transform are able to detect whole radiation beam and collect data over wide spectral range. Fourier transform is as a mathematical tool that converts the interferogram into infrared spectrum where intensity is a function of wavenumbers[93].

X-ray photoelectron spectroscopy (XPS) is non-optical technique and produces information about chemical elements in sample surface. The nature of chemical elements is revealed from characteristic photoelectrons with characteristic energy levels emitted from outer atomic layers of solid material. The emission of electrons appears as a response to incident X-ray photon that is applied on the specimen. The kinetics of the emitted electrons is detected and used to calculate their binding energies in the atom. Binding energies of atomic electrons are characteristic for each element, which enables to determine the elemental composition in the material surface. X-ray beam is produced by X-ray gun. Ion gun is applied to the materials surface clean from impurities and allow peeling of thin surface layer for depth profile measurements. Emitted electrons have to pass through set of electromagnetic lenses to concentric hemispherical sector of analyzer and detector under applied potential[93].

Diffraction methods are effective for structural analysis of material. Such techniques reflect different crystalline structures within same material chemical composition. X-ray diffractometry uses monochromatic X-ray beam which is produced in X-ray tube and filter is

used to release just single wavelength X-ray beam. Such beam is applied on sample and the diffraction of such beam on the sample crystallographic lattice is detected. Amorphous materials exhibits low interference due to random atomic distribution and orientation. On the other hand, highly crystallic materials exhibit strong interferences resulting in sharp ordered signals of its crystallographic lattice. X-ray tube, specimen and detector can change the angle with respect to each other which enables to obtain pattern of diffraction intensities in the range of used diffraction angles. Obtained peaks are depicted in range of 2θ degrees positions and characterize diffraction on specific crystallographic lattice. In diffraction pattern we can find information about crystal order/disorder, interlayer distance or atomic position. Comparison of the unknown spectrum with standard spectrum is used for qualitative analysis[93].

Last used technique is Raman spectroscopy, which is non-destructive technique useful for analysis of graphene materials, particularly number of its layers or order/disorder of material crystal lattice. To obtain Raman spectrum, pulsed laser beam is applied onto the specimen and after their interaction, photons emitted from specimen are detected. Raman spectroscopy however detects only specific, inelastic photons that are emitted in small fraction along with strong elastically scattered photons. Inelastic photons are those with changed frequency from the frequency of origin exciting photons; either have higher or lower frequency. Stokes scattering emits photons with lower energy because they are emitted by relaxation of electrons excited to higher energetic level than electron originally was. Anti-stokes scattering, on the other hand, emits photons with higher energy, since the released photons are emitted by relaxation of excited electrons onto lower energetic level, than originally were. Qualitative information about vibration levels in the molecules is detected from the shifts between laser frequencies and emitted frequencies. In graphene materials, specific bands observed are G, D and 2D bands, which corresponds to in-plane center phonon mode, phonon-defect mode and boundary phonon mode, respectively. G band reflects sp^2 carbon hybridization, D band reflects the disorder of plane into sp^3 hybridization and/or defects and 2D band refers to number of layers in the material and is affected by doping and lattice defects[93].

Such spectroscopy and microscopy analyses served for description and understanding the formation process and structure of our prepared samples. They were performed mostly in a solid phase.

5.3. Experimental setup

Electrochemical characterization

Electrochemical measurement was performed in three-electrode cell setup including working, reference and counter electrode. Silver/silver chloride (Ag/AgCl) electrode and stainless steel wire were employed as reference and counter electrodes, respectively. Glassy carbon electrodes (GCE), either bare or modified with samples were used as working electrodes. Modification process was performed by drop-coating as depicted in Figure 10a. Usually, before electrode modification, 1mg ml^{-1} aqueous dispersion of sample was shortly sonicated and then 10 µl of dispersion was dropped onto GCE surface and allowed to dry at room temperature. The whole electrochemical cell can be seen in Figure 10b. Cyclic voltammetry or electrochemical impedance spectroscopy were performed in 0.1M KCl containing 5mM $K_4Fe(CN)_6/K_3Fe(CN)_6$ (1:1) as redox probe. All electrochemical measurements were performed using a potentiostat Autolab PGSTAT 128N.

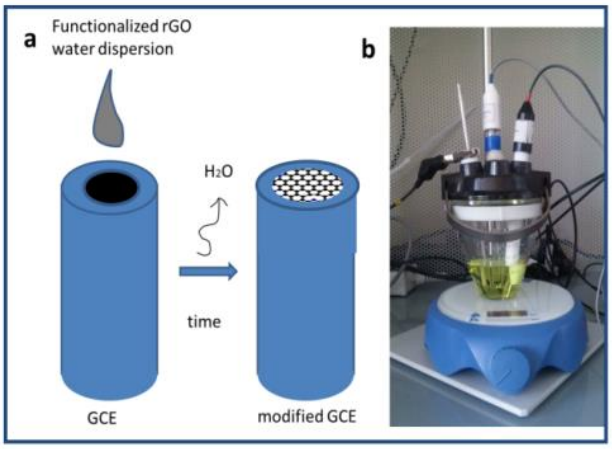

Figure 10. a) Illustration of drop-coating method used for GCE modification; b) electrochemical cell used for electrochemical measurements.

ORR measurements

ORR catalytic study was performed as well in three-electrode cell setup, although, rotation disc electrodes (RDE) was employed as working electrode (see Figure 12). Measurements were performed in both O_2-saturated and Ar-saturated 0.1M KOH as electrolyte, additional measurements in 0.5M H_2SO_4 or phosphate buffer solution at pH=7 (PBS 7) were also performed.

Catalyst ink used for working electrode modification was prepared by mixing 2 mg of sample, 196 µl water, 196 µl EtOH and 8 µl Nafion in mentioned order followed by ultrasonication for 20 minutes. As prepared catalyst ink was afterwards drop-coated (5 µl) or spin-coated (8 µl) at 600 rpm for 5 min (see Figure 11) onto the glassy carbon surface of RDE. ORR measurements were usually performed using linear sweep voltammetry (LSV) in the potential window from -0.8 to 0.2 V vs. Ag/AgCl with scan rate of 5 mV/s. Different rotation speeds ranging from 400 up to 2000 rpm were used.

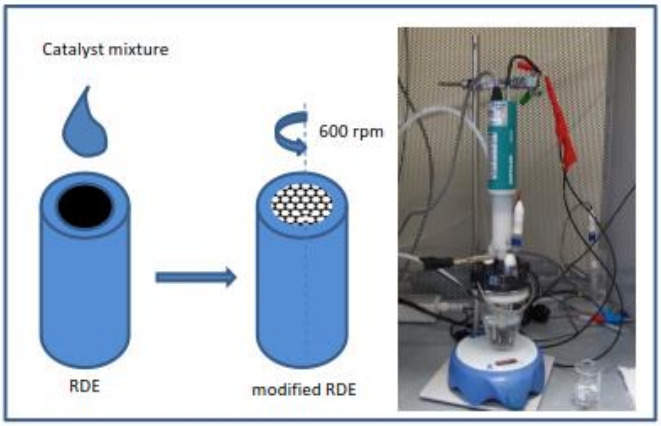

Figure 11. Illustration of spin-coating method used for RDE modification and electrochemical cell used for all catalytic measurements.

6. Results and discussion

6.1. Chemical composition and structural properties

First, GO used as starting material for all mentioned synthesis of nitrogen-doped aerogels, was thoroughly characterized for better understanding of further nitrogen doping. SEM and TEM images revealed nearly transparent, crumpled single layered sheets of GO as can be seen in Figure 12a-b. This finding confirmed that high quality starting material was obtained following the Hummer´s method of synthesis. FTIR analysis (Figure 12c) confirmed high degree of oxidation reflected by main absorption band assigned to hydroxyl groups stretching vibration (3411 cm^{-1}), C=O stretching of carboxylic groups (1711 cm^{-1}), C-O stretching of epoxy and/or alkoxy vibrations occurred in the region between 1000 and 1300 cm^{-1} in addition to C=C vibration at 1626 cm^{-1} [91]. Such finding is in agreement with restoration of graphite layers into oxidized GO sheets. XRD pattern depicted in Figure 12d.

showed characteristic graphitic peak at 2θ = 31° with interlayer spacing of 0.34 Å in the case of graphite. In contrast, GO exhibited typical diffraction peak at 2θ = 13.01° [91] with interlayer spacing of 7.72 Å, which is 2 times higher than interlayer distance in graphite which verified successful exfoliation of graphite sheets during the oxidation process.

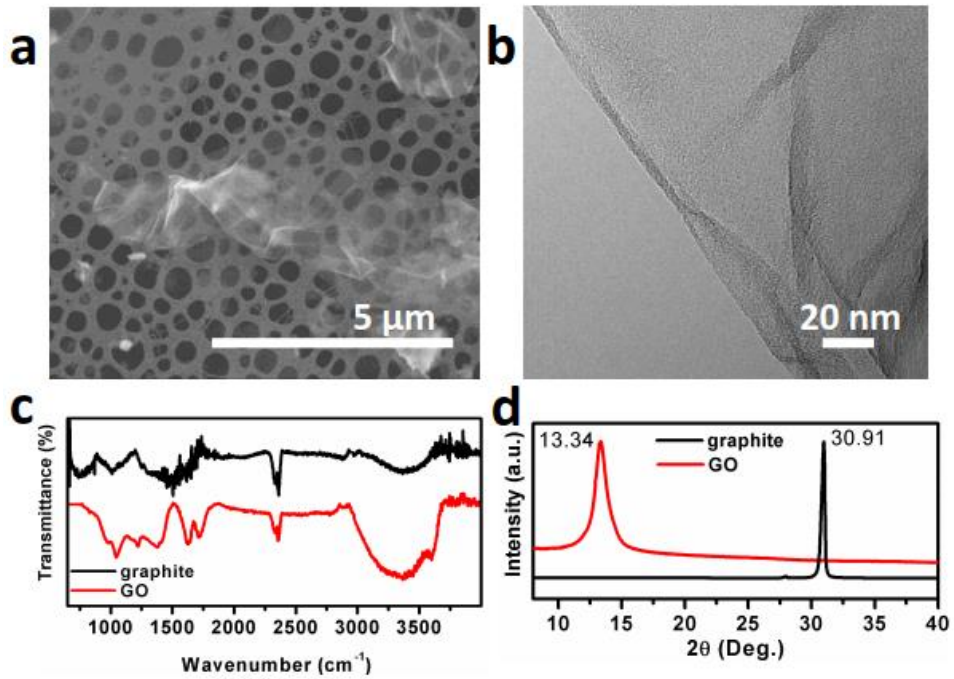

Figure 12. a) SEM image of GO nanosheet, b) TEM image of GO nanosheet, c) FTIR spectrum of graphite (black) and GO nanosheet (red) and d) X-ray powder diffraction patterns of graphite (black) and GO nanosheet (red).

Nitrogen-doped reduced graphene oxide aerogels (GA-N)

Nitrogen doping was performed via simple hydrothermal method during which the GO precursor and nitrogen source were mixed and underwent hydrothermal treatment at 180 °C. This allowed self-assembling into 3D hydrogel structure which was achieved by reaction between oxygen containing functional groups of GO and nitrogen molecules. Therefore, reduction of GO, doping with nitrogen and formation of 3D architecture was simply reached in one pot synthesis. Intentionally, there were chosen 4 different N precursors differing in chemical composition and content to see the effect of N precursor on the ORR catalysis performance and to test the hypothesis of precursor-controlled nitrogen configuration. While two diamines were represented by aliphatic and aromatic diamine in para position (ethylenediamine, p-phenylenediamine), there was also chosen polymer - 5-membered ring with carbonyl group and vinyl monomer character with average mol wt 10 000

(poly(vinyl)pyrrolidone) and finally widely used ammonium hydroxide (NH_4OH) as representative of simple monoamine.

Diverse structural properties of four nitrogen-doped samples are reflected in the SEM images in Figure 14. One can distinguish some degree of porous-like structure (Figure 13a, GA-N(EDA)), either less organized (Fig. 13b, GA-N(pPDA)) or densed, more bulky organization (Fig. 14c, GA-N(PVP)).

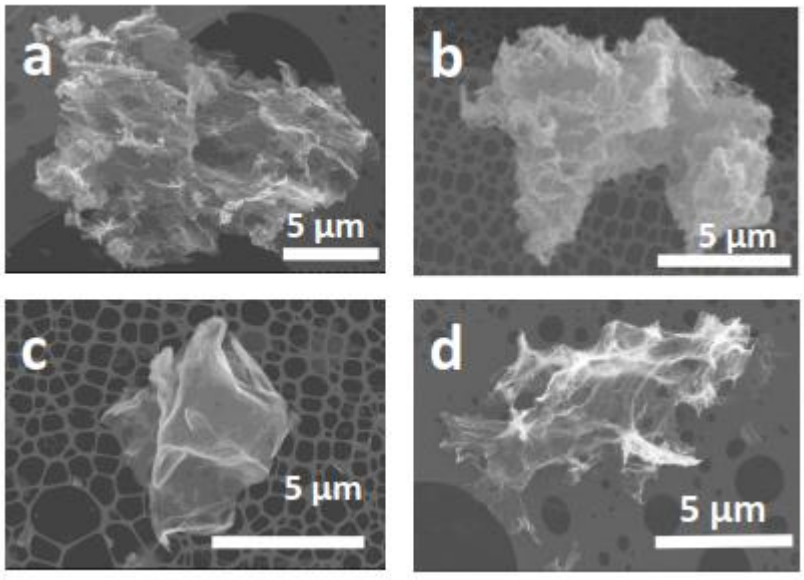

Figure 13. SEM images of GA-N(pPDA), GA-N(PVP), GA-N(NH4OH) and GA-N(EDA 3:1).

In contrast, completely different structure with no obvious porosity was observed for GA-N(NH_4OH) in Fig.14d. This was probably caused by different synthesis conditions, as this was the only sample prepared by chemical reduction at much lower temperature and shorter reaction time than the hydrothermal treatment used for other samples. For this reason we might presume that only partial reduction of GO appeared.

The TEM images of all samples are summarized in Figure 14. In all cases, large transparent single nanosheets were observed, that were folded. Such folding is typical feature of graphene sheets with finite size[94]. Crooked character is result of hot and wet reaction conditions which is observed in all samples.

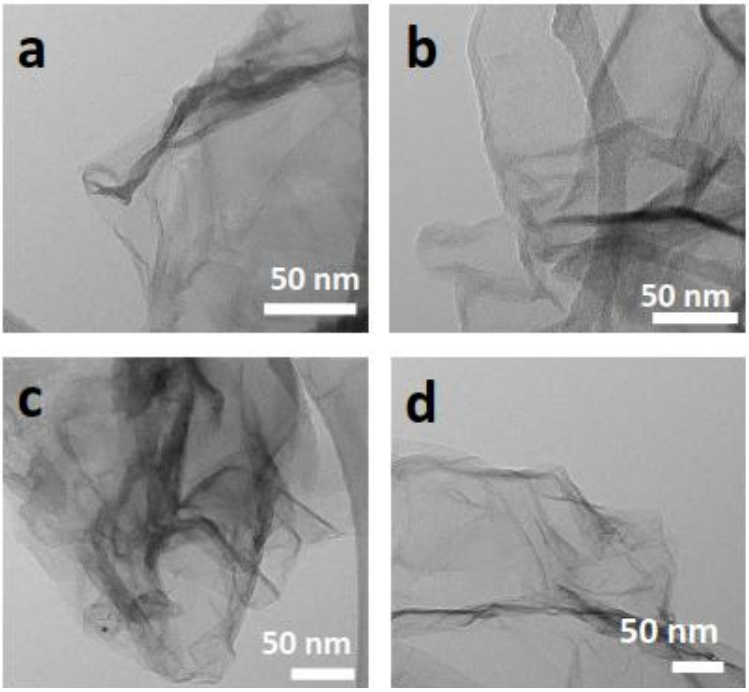

Figure 14. TEM images of GA-N(pPDA), GA-N(PVP), GA-N(NH_4OH) and GA-N(EDA 3:1).

Finally, one can see photographs showing well-defined cylindrical-shape of final hydrogel and aerogel samples (Figure 15). Their size varied between 2 and 2.5 cm. All aerogels were very light indicating thus high porous-like structure. As one can expect, the only difference in morphology was observed for GA-N(NH_4OH) sample from obvious reason mentioned above.

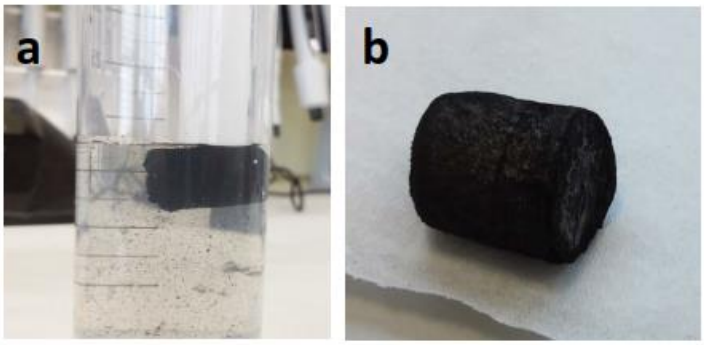

Figure 15. a) Photo of hydrothermally prepared GH-N hydrogel; b) photo of GA-N aerogel obtained after freeze-drying of GH-N hydrogel.

Fourier-transform infer-red spectroscopy (FT-IR) was performed in order to see the degree of reduction and character of oxygen functional groups remaining on the surface of sample (see Figure 16). Reduction of the sample was obvious from of hydroxyl group stretching vibration (~3400 cm^{-1}) that disappeared in nitrogen-doped samples (*i.e.*, GA-

N(EDA), GA-N(pPDA), GA-N(NH_4OH) compared to GO. The exception behavior was observed with sample GA-N(PVP) that possessed still hydroxyl functional groups even after hydrothermal treatment. Surprising was however its stronger OH mode than has GO itself. This meant that GA-N(PVP) source molecule did not attack O-functionalities on GO surface or moreover it correlated with the content of its own surface oxygen group.

Successful reduction process was also reflected by downshifting of carboxyl vibration band to 1701 cm^{-1} and 1665 cm^{-1} observed for GA-N(EDA), GA-N(pPDA) and GA-N(NH_4OH), respectively, compare to GO (1723 cm^{-1}). This fact demonstrated additional functionalization into C-N bond. Even higher downshifting could be seen in case of GA-N(PVP) (1643 cm^{-1}) characterizing probably further change of C=O vibrations into C=N bond in the pyrrolic ring. Successful functionalization of GA-N(NH_4OH) then could be seen in peak at 3270 cm^{-1} representing the N-H stretching vibrations[95].

C=C stretching vibration was negatively shifted for nitrogen-doped samples compared to GO, suggesting the restoration of conjugated network by reduction since same trend was observed for un-doped GA. Finally, peaks region between 1000 – 1300 cm^{-1} was observed in all functionalized samples. The broadness of this peak characterizing C-N/N-H vibration bands thus indicated reaction between surface epoxy and hydroxyl functional groups of GO with N molecules[95,96]. Similarly, C-O at 1050 cm^{-1} [95], could be also observed since some doped samples (*i.e.*, GA-N(PVP) and GA-N(NH_4OH)) contained some of oxygen surface functional groups that remained from GO structure as the result of imperfect reduction process as described above. This vibration band was not observed in the case of fully reduced samples (*i.e.*, GA-N(pPDA) and GA-N(EDA)).

In summary, all above mentioned results obtained from FT-IR analysis thus proved the successful reduction of oxygen surface functional groups of starting material (*i.e.*, GO) and their functionalization with nitrogen in all samples produced in this research work, even though that the degree of reduction varies between the samples.

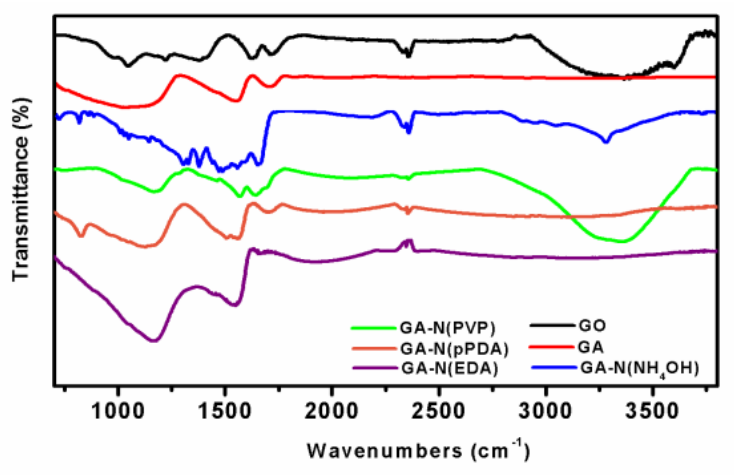

Figure 16. FTIR spectra of GO (black), GA (red) and doped samples GA-N(pPDA) (orange), GA-N(PVP) (green), GA-N(EDA) (purple) and GA-N(NH_4OH) (blue).

Following X-ray photoelectron spectroscopy (XPS) analysis clarified character of chemical elements by determining bonding states of the material atoms. Survey and high resolution N 1s spectra for all four catalysts are summarized in Figure 17, and distinguish the changes in nitrogen configuration according to the nitrogen precursor used. While GA-N(PVP) sample contained only pyrrolic N bonding state, GA-N(EDA) and GA-N(pPDA) had in their structure pyrrolic and pyridinic N, and GA-N(NH_4OH) sample consisted of amine and graphitic N. The same composition of GA-N(EDA) and GA-N(pPDA) could be attributed to the chemically similar composition of diamine.

The survey spectra depicted the composition ratio between carbon, oxygen and nitrogen, which was also varied for each sample. Interestingly, GA-N(NH_4OH) contained the highest amount of nitrogen (22.1at%). On the other hand, GA-N(PVP) was poor in nitrogen, having only 0.8at% of nitrogen inside. GA-N(EDA) and GA-N(pPDA) again revealed analogous results with similar nitrogen contents of 6.6 and 5.8at%, respectively. The differences in the nitrogen compositions between samples could be attributed probably to specificity of the precursor itself, its chemical structure and composition.

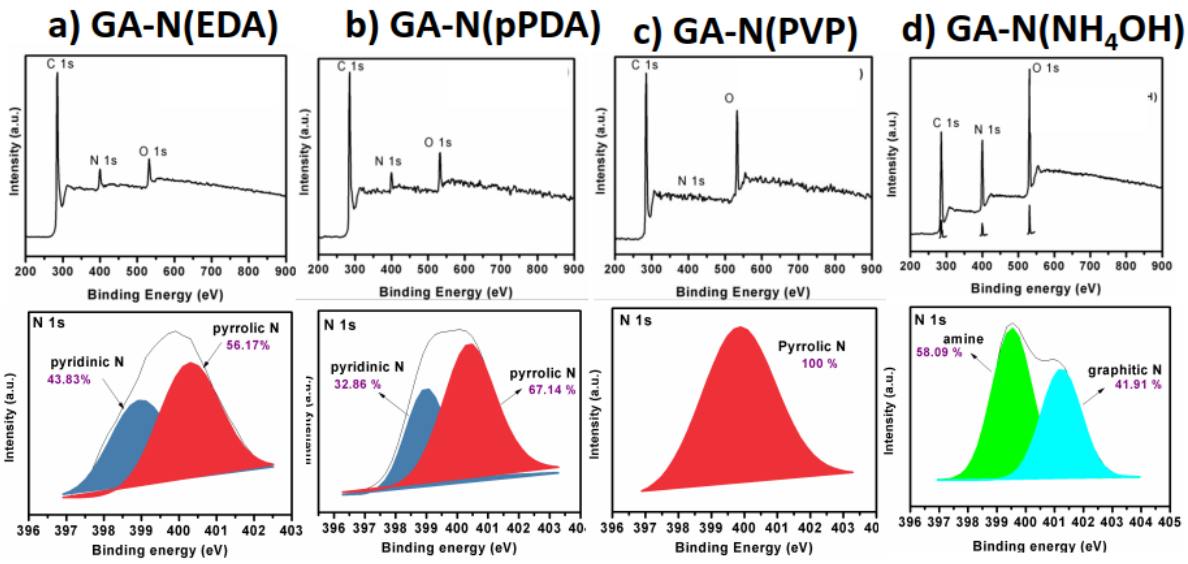

Figure 17. XPS analysis of GA-N samples. Survey spectra (up) and deconvoluted high resolution N 1s spectra (down) of: a) GA-N(EDA); b) GA-N(pPDA); c) GA-N(PVP); d) GA-N(NH_4OH).

6.2. Electrochemical characterization

To address the electro-activity of prepared samples, basic electrochemical characterization was performed, including cyclic voltammetry and electrochemical impedance spectroscopy.

Comparison of cyclic voltammograms (see Figure 18a) performed at scan rate of 50 mV/s illustrated that after deposition of all doped GA samples onto glassy carbon electrode (GCE), peak current response to the redox system (*i.e.* $[Fe(CN)_6]^{3-/4-}$) was significantly increased, in contrast to GCE modified with pure GO. Reduction of GO was here clearly proved as necessary route towards making material (more) electro-active. Modification with samples GA-N(EDA) and GA-N(pPDA) demonstrated more rectangular shape of the voltammogram in contrast to other two samples, corresponding to better conductivity of these samples as well as to higher electro-active area. The decrease of the current response in case of GA-N(PVP) and GA-N(NH_4OH) samples might result from significantly higher oxygen content on the sample surface which decreased their conductivity.

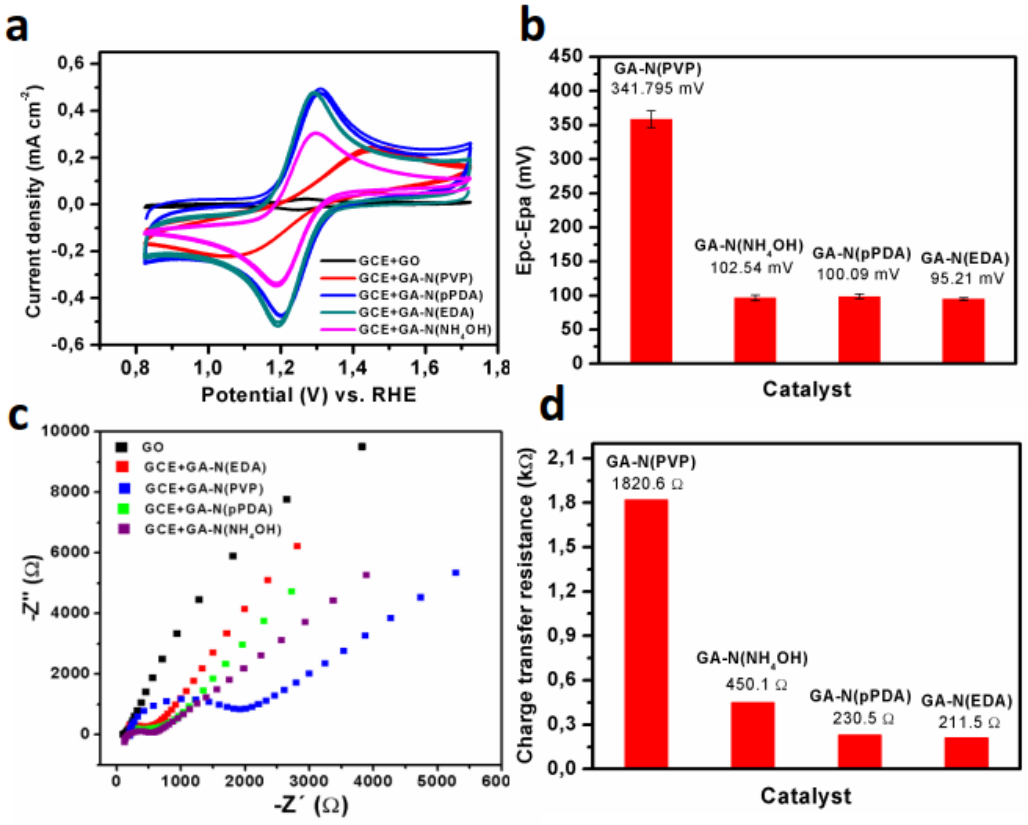

Figure 18. Electrochemical performance of GA-N samples measured in 0.1M KOH. a) Cyclic voltammograms recorded at scan rate of 50 mV/s with GCE modified with GO (black), GA-N(pPDA) (blue), GA-N(PVP) (red), GA-N(EDA) (green) and GA-N(NH_4OH) (pink); b) Peak-to-peak separation obtained with different modified GCE; c) EIS measurements for GCE modified with GO (black), GA-N(PVP) (blue), GA-N(pPDA) (green), GA-N(EDA) (red) and GA-N(NH_4OH) (purple); d) Graph of charge transfer resistance (R_{ct}) recorded with the EIS measurement and obtained by fitting with equivalent Randles circuit.

The peak-to-peak potential separation ($\Delta E = E_{pa} - E_{pc}$) calculated for each sample at 50 mV/s are shown in Figure 18b. Such value can be used to demonstrate individual electron transfer rates. Since the theoretical value of ΔE for ideally fast and reversible redox reaction of used system is 59 mV (from Nernst equation), desire is to obtain the ΔE value the closest to 59 mV as possible. However, in real electrochemical systems, such value is nearly unreachable. Calculated values, in our case, demonstrated that the most reversible reaction occured on the electrode modified with GA-N(EDA) with ΔE = 95.21 mV. The worst ΔE value of 342 mV was observed on the electrode modified with GA-N(PVP). On the other hand, it should be highlighted that GA-N(EDA), GA-N(pPDA) and also GA-N(NH_4OH) samples anyway enhanced the electrochemical performance of bare GCE (ΔE = 120 mV). Scan rate study was also performed in order to verify kinetics of the electron transfer of modified electrodes. Set of voltammetry measurements for each sample were performed in the

range of scan rates from 30 to 200 mV/s (not shown). All samples exhibited linear relationship between the square root of scan rate and peak current response. Redox reaction occurring at all the electrode/electrolyte interfaces was therefore evaluated as diffusion-controlled.

The electron transfer properties were further characterized by electrochemical impedance spectroscopy (EIS). It can be seen in Nyquist plots depicted in Figure 18c, that aerogel-like electrode surface of the samples substantially decreased the charge transfer resistance in contrast to pure GO modified electrode, as can be seen from smaller or even disappearance of semi-circle of Nyquist plot compare to GO. EIS measurements were consistent with CV measurements of modified electrodes and thus proving that all samples were more conductive than GO. Value of charge transfer resistance (R_{ct}) was obtained by fitting the Nyquist plot according to equivalent Randles circuit ([R(Q[RW])]). Among all doped samples, the highest charge transfer resistance was measured for GA-N(PVP) (1820.6 Ω, Figure 18d) and corresponded to very poor quality and reversibility of the performed reaction demonstrated by CV measurement.

In summary, we observed that GA-N(EDA) and GA-N(pPDA) samples possessed the most enhanced electro-catalytic properties. SEM and TEM images revealed expanded architecture of these samples that could be beneficial for enhanced electrolyte diffusion, which in turn led to enhanced capacitive current and significantly reduced electron transfer resistance compare to GO.

6.3. ORR catalytic study

Application of four samples in catalysis of ORR brought results that are shown in Figure 19. Differences between samples used for rotation disc electrode (RDE) modification could be seen in both onset potential and current peak intensity (see Figure 19a). N-doped GA samples exhibited higher catalytic activity than pure GO, which showed nearly no reduction peak. However, all modifications showed lower catalytic activity than commercially available Pt/C catalyst, nevertheless, to obtain superior activities was not an object of this thesis. Our aim was to define how the structure and type of nitrogen precursor of GA-N samples influenced the ORR catalytic properties of such samples.

RDE modified with GA-N(PVP) and GA-N(NH_4OH) sample exhibited the worst results in the term of the highest over-potential (*i.e.* 0.757 V and 0.715 V vs. RHE, respectively) and low current density. Much better parameters (*i.e.* lower over-potential and increased current density) was observed in case of GA-N(pPDA). Nonetheless, all mentioned samples exhibited highly damaged S-shaped LSV curve which was rather indicative of inactive catalyst material toward ORR. Ideal curve was however observed for electrodes modified by GA-N(EDA). Optimal shape, one of the lowest over-potential and high current intensity unambiguously determined GA-N(EDA) as the most successful catalyst material from all doped samples. The center part of the curve of GA-N(EDA) modified RDE was parallel with that of Pt/C modified electrode, referring to optimal catalytic process.

Comparison of onset potentials measured on modified electrodes are highlighted in Figure 19b, The best onset potential was measured with electrode modified with GA-N(EDA) (0.825 V) and GA-N(pPDA) (0.860 V) since these values was the closest to the onset potential of electrode modified with commercial Pt/C catalyst.

LSV voltammograms were also performed under the same conditions in Ar-saturated electrolyte which showed no ORR activity at all and were clear evidence of catalytic activities towards ORR of tested samples.

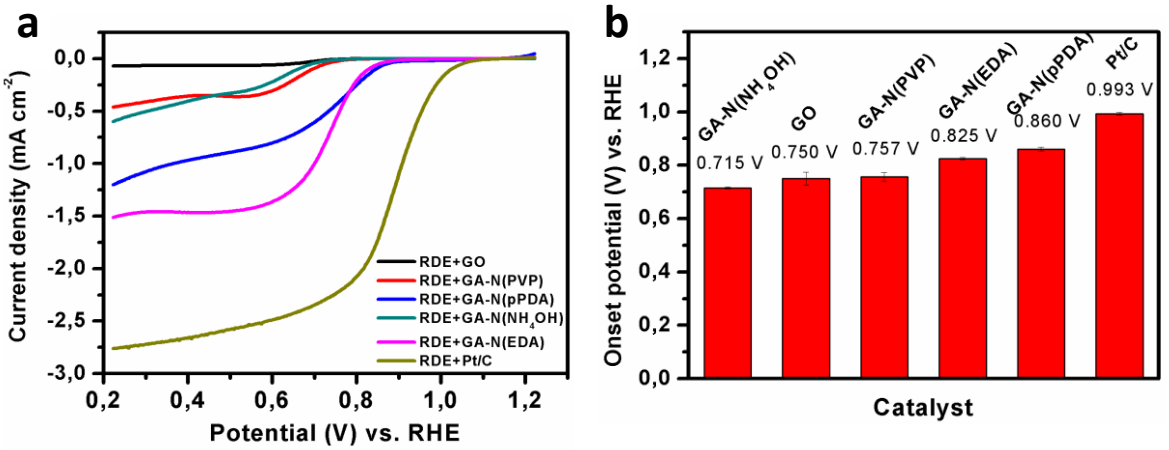

Figure 19. a) Linear sweep voltammograms recorded in O_2-saturated 0.1M KOH with RDE modified with GO (black), GA-N(pPDA) (blue), GA-N(PVP) (red), GA-N(EDA) (pink), GA-N(NH_4OH) (green) and Pt/C catalyst (khaki); b) comparison of onset potentials for modified electrodes corresponding to LSV measurement.

Taking all results together, the catalytic activity was specifically affected by the nature of the nitrogen precursor and the curve shape was an indicator of the ink quality of the modification, which has also effect on catalytic performance.

Due to evaluation of GA-N(EDA) sample as the most promising toward ORR, we decided to perform more optimization regarding this sample. Especially, we focused on GO:EDA ratio used during the synthesis and its subsequent effect on ORR catalytic activity. There were prepared samples containing three different GO:EDA ratios: to the initial ratio 3:1, ratios 1:1 and 1:3 were also studied and their characterization is shown hereafter.

6.4. Effect of different GO:EDA ratio to the sample composition

In order to analyze sample composition, XPS spectra of samples with different GO:EDA ratios were analyzed. XPS O 1s spectra (not shown) were basically same for all samples, introducing half C-O and half C=O bond representative. In the similar manner, C 1s spectra (not shown) indicated that all four samples were formed in majority of C-C bond in sp^2 hybridization (~60%), while the content of defects (C in sp^3 hybridization) were present in lower amount (around 11-14%). Following groups included C-O/C-N bonding and residual of carboxyl C=O groups. Most important qualitative variance between samples was illustrated in high resolution N 1s spectra. While GA-N(EDA 1:3) was functionalized by only pyrrolic N, in case of GA-N(EDA 3:1) nitrogen content was depicted as majority of pyrrolic N and also minor amount pyridinic N. Sample GA-N(EDA 1:1) was doped with three types of N, in decreasing order pyrrolic, pyridinic and graphitic N. This was an evidence of the fact that specific GO:EDA ratio could influence the formation of different nitrogen configurations.

Effect of the reaction time

In order to see the effect of reaction time change on the EDA incorporation, there was prepared sample GA-N(EDA 1:1) also in shorter reaction time of 3 hours, apart from usual 12-hour reaction. Such treated sample (GA-N(EDA 1:1)3h) contained only pyrrolic N, in contrast to graphitic, pyrrolic and pyridinic N in GA-N(EDA 1:1). It is also worth to note that both samples with GO:EDA 1:1 ratio were quantitatively comparable when speaking about nitrogen content presented after functionalization process. Based on this experiment, it could be assumed that formation of pyridinic and graphitic N probably needed specific time. Actually, time-dependency of N-type formation was already observed in hydrothermal

treatment[97]. Anyway, further and repeated synthesis and testing of more reaction times should be monitored for better understanding of this effect, but due to the limited time it was not performed in this thesis.

6.4.1. Chemical composition and structural properties

As we obtained new group of catalysts (*i.e.*, GA-N(EDA) with different ratio GO:EDA during the synthesis procedure), we performed their chemical and structural analysis once again. Comparison of samples morphology is depicted in SEM and TEM images. Porous-like structure resulted from hydrothermal treatment could be seen for all samples in SEM images (Figure 20). High-volume structures with significantly expanded GO sheets were obvious in images a-d, while higher magnification revealed their details in images e-h. TEM images in Figure 21 depicted transparent sheets of N-doped GA of prepared samples, indicating that the sheets were single-layered.

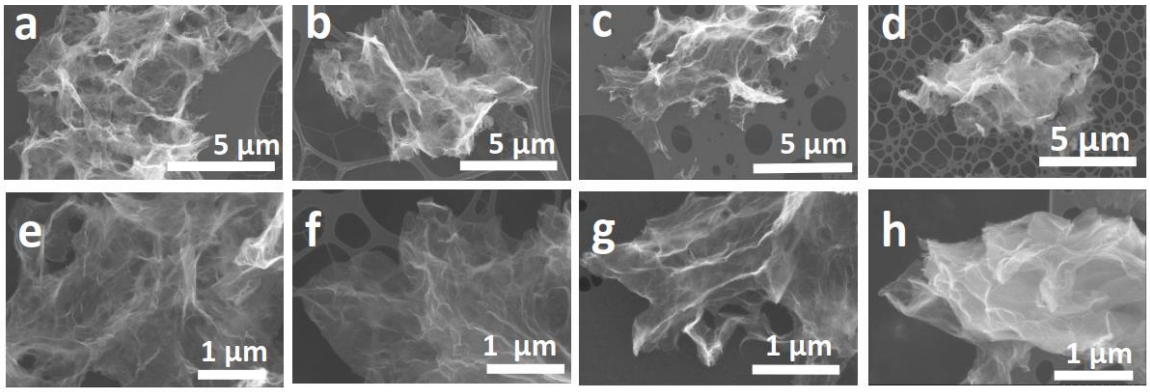

Figure 20. SEM images of a,e) GA-N(1:1); b,f) GA-N(1:1)3h; c,g) GA-N(EDA 3:1) and d,h) GA-N(EDA 1:3).

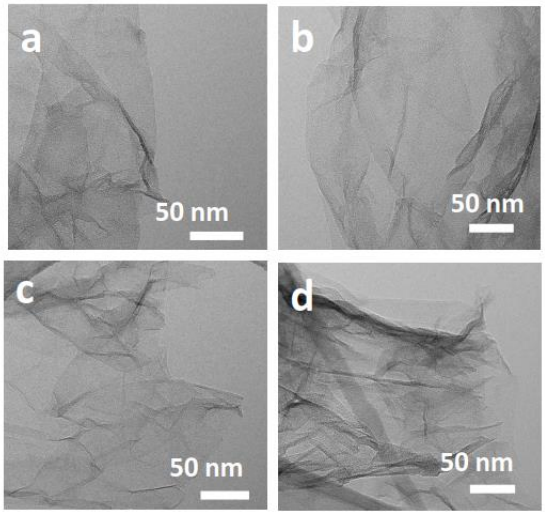

Figure 21. TEM images of a) GA-N(1:1); b) GA-N(1:1)3h; c) GA-N(EDA 3:1) and d) GA-N(EDA 1:3).

From the composition point of view, the highest nitrogen content in final sample was 8.4at% according to XPS analysis, and this value belonged to sample with ratio GA-N(EDA 1:1)3h, with further decreasing content from GA-N(EDA 1:1), GA-N(EDA 3:1) to GA-N(EDA 1:3) with percentages of 8.1, 6.6 and 6.5at%, respectively.

Comparison of chemical bonding is depicted in FT-IR spectra in Figure 22. Successful functionalization with nitrogen could be seen in the range between 1000 cm^{-1} and 1360 cm^{-1} which indicated presence of C-N/N-H vibrating mode in all samples.

However, incomplete reduction of GO was obvious at spectra of GA-N(EDA 1:1)3h and GA-N(EDA 1:3) samples, where there were substantial residues of OH (3400 cm^{-1}) and C=O (1665 cm^{-1}) surface groups. For GA-N(EDA 1:1)3h, this fact was indicative of insufficient reduction time, however in the case of GA-N(EDA1:3) this argument could not be used and therefore it was attributed to another unknown condition.

Samples GA-N(EDA 1:1) and GA-N(EDA 3:1) unambiguously differed from the other two samples by highly reduced surface oxygen groups. Due to this observation, they were promising candidates for enhanced electro-catalytic activities.

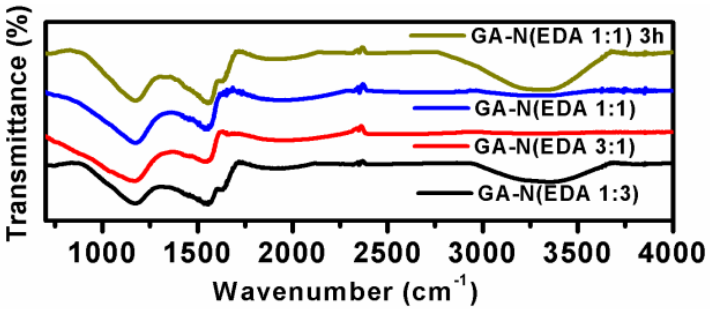

Figure 22. FTIR spectra of GA-N(EDA 3:1) (red), GA-N(EDA 1:3) (black), GA-N(EDA 1:1) (blue) and GA-N(EDA 1:1)3h (green).

Raman spectroscopy analysis was performed in order to demonstrate the degree of defects and doping in GA-N(EDA) samples. Raman spectra are depicted in Figure 23, where typical graphene signs could be seen in G and D band at 1591 cm^{-1} and 1325 cm^{-1}, respectively. G band was related to graphitic in-plane structure in GA network and D band, characteristic for sp^3 carbon hybridization, was related to the reduction of surface oxygen species of GO and attachment or incorporation of nitrogen atoms into the GA lattice.

Illustration of sample defects is usually demonstrated by intensity ratio between D and G band (I_D/I_G ratio). For our samples, I_D/I_G ratios exhibited similar values, particularly 1.51, 1.48, 1.50 and 1.43 for GA-N(EDA 1:1), GA-N(EDA 1:1)3h, GA-N(EDA 3:1) and GA-N(EDA 1:3), respectively. This was in agreement with logical presumption of higher concentration of defects in doped samples than in un-doped GO (I_D/I_G = 0.96).

Another sign of doping could be seen when focusing on the bands position. We could observe that D band remained unchanged for all doped samples and GO, whereas G band was upper-shifted in doped samples (1591 cm^{-1}) in contrast to un-doped GO (1561 cm^{-1}), which is typical for nitrogen doping as it results from distortion of sp^2 network by reaction of surface oxygen with nitrogen molecules[55,98,99].

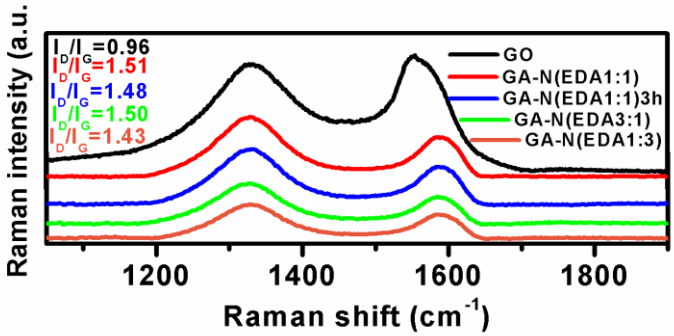

Figure 23. Raman spectra of samples GO (black), GA-N(EDA 3:1) (green), GA-N(EDA 1:3) (orange), GA-N(EDA 1:1) (red) and GA-N(EDA 1:1)3h (blue).

6.4.2. Electrochemical characterization

Another set of basic electrochemical characterization was employed to observe electro-activity of all GA-N(EDA) samples. Cyclic voltammetry was performed under the same conditions as previous samples, in 0.1M KCl. Enhanced electrochemical response to redox system compare to un-doped GO or bare GCE, high reversibility of the occurred redox reaction as well as good response in scan rate study and diffusion study was observed for all doped samples. This was demonstrated by linear increment of peak current responses with increment of scan rate and proportional increment of peak current with square root of scan rate, indicating that reaction on the electrode/electrolyte interface was controlled by diffusion. Enhanced activity using GA-N(EDA 3:1) for electrode modification compare to other modified electrodes was observed in peak current response, whereas in reversibility tests the best result (89.8 mV) exhibited GA-N(EDA 1:1) sample (see Figure 24).

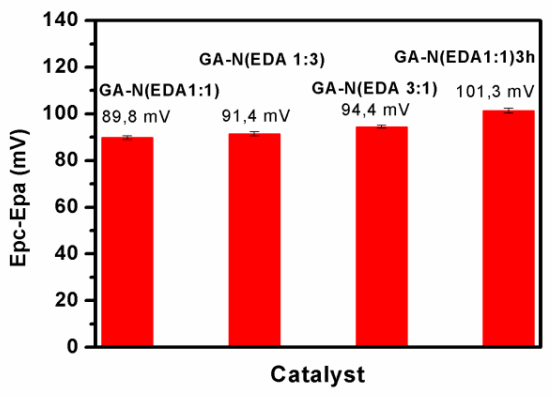

Figure 24. Graph of ΔE values for GCE modified with GA-N(EDA 3:1), GA-N(EDA 1:3), GA-N(EDA 1:1) and GA-N(EDA 1:1)3h.

In summary, all prepared samples with different GO:EDA ratios were doped by nitrogen in comparable amount and exhibited expanded porous-like structures, which resulted in enhanced electrochemical response in studied system.

6.3.4. ORR catalytic study and optimization

In order to see how the differences in prepared samples (especially nitrogen configuration) influence the ORR catalysis, final ORR testing was performed. As in previous testing, there was employed O_2-saturated and Ar-saturated 0.1M KOH electrolyte, also catalyst inks were prepared by the same method. ORR results with corresponding XPS N1s spectra are summarized in Figure 25.

The highest catalytic activity towards ORR and very good activity was observed in case of the two best samples - GA-N(EDA 3:1) and second GA-N(EDA 1:1), which was in correspondence with previous characterizations revealing these two samples most similar to each other and most reduced. The onset potential of GA-N(EDA 3:1) and GA-N(EDA 1:1) were 0.84 V and 0.82 V vs. RHE, respectively. Current densities for GA-N(EDA 3:1) and GA-N(EDA 1:1) were 1.5 mA cm^{-2} and 1.35 mA cm^{-2}, respectively.

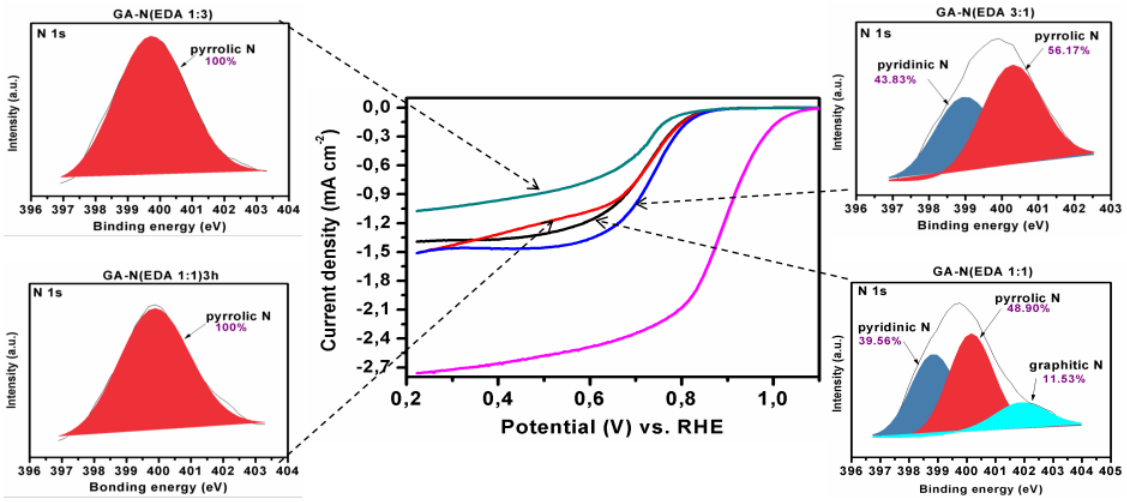

Figure 25. Linear sweep voltammograms recorded in 0.1M KOH saturated with O_2 with RDE modified by GA-N(EDA 3:1) (blue), GA-N(EDA 1:3) (green), GA-N(EDA 1:1) (black), GA-N(EDA 1:1)3h (red) and Pt/C catalyst (pink) with corresponding high resolution N 1s spectra from XPS analysis.

On the other hand, unsuitability of GA-N(EDA 1:3) and GA-N(EDA 1:1)3h samples was also confirmed, due to high oxygen content in the material. This could be demonstrated by deficient shape of the LSV curve and explained by reduction of its own surface oxygen functionalities and hindering the actual reduction of oxygen in the electrolyte, which is the purpose of the reaction. To elucidate which type of reduction actually occurred on the GA-N(EDA 1:3) and GA-N(EDA 1:1)3h electrodes, these samples were subjected to CV measurement in pure 0.5M KCl without redox couple (data not shown). Indeed, there was observed reduction peak at the same onset potential as reduction peak observed in O_2-saturated KOH, thus, it was proved that at least some part of the LSV peak was produced by reduction of its own surface oxygen groups. The same result were obtained also for GA-N(PVP) or GA-N(pPDA) which also did not worked well in previous ORR catalysis tests.

The assumption that promised GA-N(EDA 3:1) sample as the best candidate for ORR catalysis was proved by best onset potential and best current intensity obtained by LSV measurements. Enhancement in activities was attributed to the content of pyrrolic and pyridinic N incorporated within the structure via most optimal ratio of reaction components, GO and EDA. In this light, GA-N(EDA 3:1) was used for further ORR measurement optimization.

Catalytic properties of GA-N(EDA 3:1) in different media

Nowadays, there are newly developed metal-free catalysts that possess advanced catalytic properties, sometimes even overcoming those of Pt/C[48]. Nevertheless, in majority of cases they demonstrate good results only in specific medium, especially graphene-based catalysts commonly work in alkaline media[2,52].

The good response of GA-N(EDA 3:1) as catalyst in alkaline medium motivated us to try its abilities also in different types of media, in neutral (phosphate buffer solution at pH=7) and acidic one (0.5M H_2SO_4). Surprisingly, GA-N(EDA 3:1) was able to catalyze ORR in all three kinds of media, as commercial Pt/C, although in lowered activities. In all electrolytes, GA-N(EDA 3:1) exhibited larger over-potential in contrast to Pt/C catalysts, yet the universal utility of such metal-free simple and cost-effective catalyst was highly positive.

Further electro-catalytic and kinetic study of GA-N(EDA 3:1) included measurement of LSV curves at different rotating rates, which is depicted in Figure 26. LSV curves demonstrated linear increase of catalytic current with rotating rate increasing from 400 to 2000 rpm which was indicative of good catalyst function toward ORR.

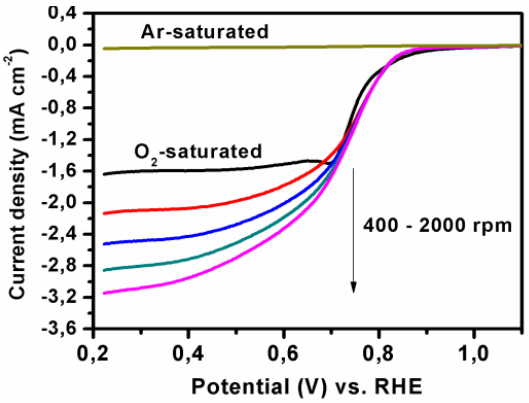

Figure 26. Linear sweep voltammograms recorded with RDE modified by GA-N(EDA 3:1) in 0.1M KOH at rotation speeds 400, 800, 1200, 1600 and 2000 rpm.

6.4.3. Catalyst ink formation optimization

Due to partial inhomogeneity and/or non-uniformity of the GA-N(EDA) inks, there was conducted another measurement with modified ways of ink formations in order to obtain better and controllable response. The role of the catalyst ink quality is huge and general rule is

the more uniform and homogeneous ink is formed, the better conditions for process at the electrode surface are facilitated.

The used drop-coating method of ink formation is the easiest one, however it was found unsuitable for our hydrophobic materials which tended to aggregate during the drying process on the electrode surface. As a consequence, the catalyst ink consisted of aggregated spots which did not cover the whole active electrode area and usually tended to dry in various layers, forming the surface relief heterogeneous.

To improve the uniformity of the catalyst ink there was employed spin-coating method for electrode modification. In typical process, the solution of catalyst mixture was dropped onto the electrode surface and the electrode was then rotated, under specific rotation speed, to force the catalyst uniformly expand on the whole electrode surface. Because the catalyst ink was outspread indeed on nearly whole area of the electrode, it was necessary to drop higher amount of the catalyst to perform sufficient and perfect coverage of the electrode active area.

The optimal conditions were established to amount of 8 µl of catalyst mixture and 5 minutes of rotation at 600 rpm for spreading the catalyst and then allowed to fully dry at room temperature. The spin-coating method enabled to prepare much uniform, smoother catalyst ink film over the electrode surface, which was easily observed with the eye (see insets in Figure 27.). When used for catalysis of ORR in O_2-saturated 0.1M KOH, the difference was also obvious in substantially enhanced current density compare to drop-coated electrode. The evidence could be seen in LSV curves obtained for GA-N(EDA 3:1) catalyst in the Figure 27.

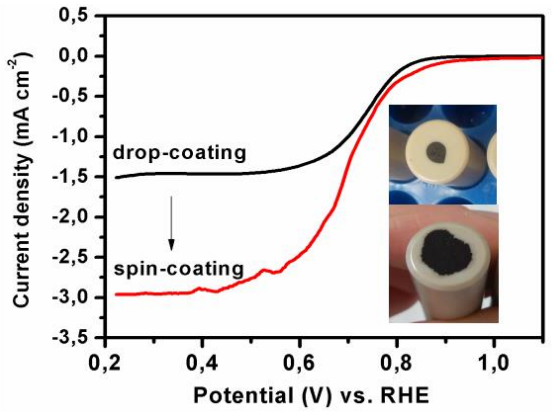

Figure 27. Linear sweep voltammograms recorded with RDE modified with GA-N(EDA 3:1) in 0.1M KOH electrolyte saturated with O_2 by drop-coating and spin-coating method. Insets: photos of catalyst ink films for each modification method.

In summary, the best result of our catalytic study exhibited the sample GA-N(EDA 3:1). Through sets of characterizations, electrochemical testing, syntheses and catalyst ink-formation optimizations there were understood some critical patterns influencing the structure and properties of hydrothermally prepared N-doped graphene-based catalytic materials.

Doping graphene with nitrogen by hydrothermal treatment apart from that is easy nature provided opportunities of controlling and tuning the final nanomaterial properties. Controlling of the synthesis including the option of nitrogen precursor and moreover the choice of ratio between nitrogen and graphene precursor played significant role in the electro-catalytic properties of final nanomaterial. Such optimization was able to influence the nitrogen configuration presented in final nanomaterial and degree of reduction of oxygen surface species, which was demonstrated by FT-IR, XPS and Raman spectroscopy. Such modification subsequently caused differences in electrochemical response, conductivity and facilitated electron transfer when used as modification for GCE. Finally, ORR catalytic activities of the samples were changed accordingly, particularly in onset potentials and current densities.

The quality of the catalyst ink, especially of its uniformity had also relevant effect on catalytic. The route of electrode modification itself could be controlled and optimized to provide even advanced activities in actual application, highlighting spin coating method as efficient for GA-N catalysts.

Summary

The aim of this work was to control the hydrothermal synthesis of nitrogen-doped reduced graphene aerogels (GA-N) by changing reaction conditions in order to obtain different nitrogen configurations and compare their electro-catalytic activities towards oxygen reduction reaction (ORR). Graphene oxide (GO) and four different nitrogen containing molecules (*i.e.,* ethylenediamine (EDA), *p*-phenylenediamine (pPDA), polyvinylpyrrolidone (PVP) and ammonium hydroxide (NH_4OH)) were used as precursors.

The detailed sample characterization confirmed successful reduction of GO to graphene aerogel (GA) and its further functionalization with nitrogen dopants. The effect of N doping was reflected in the different reduction degree in final nanomaterial as well as in electrical conductivity and enhancement of the electron transfer in tested redox system. As the most electro-catalytically active toward ORR was evaluated sample GA-N(EDA), in terms of both the onset potential and current density.

Conditions affecting the synthesis included apart from the nature of nitrogen precursor also the amount of nitrogen precursor in contrast to graphene precursor (GO:EDA = 1:1, 3:1 and 1:3). Such optimization influenced the type of nitrogen configuration presented in final nanomaterials and degree of reduction of surface oxygen species of initial graphene oxide. From all our tested samples, when modified on rotating disc electrode (RDE), the GA-N(EDA 3:1) exhibited the highest electro-catalytic response toward ORR.

The most expanded structure and highest degree of reduction of GA-N(EDA 3:1) sample has mirrored in higher capacitive current and current density, while the constitution of pyridinic and pyrrolic N in GA-N(EDA 3:1) has mirrored in highest peak current response in CV and onset potential in LSV catalytic curve. Thus, pyridinic and pyrrolic N acted as the active promotors of ORR in prepared GA-N aerogels. In addition, such doped GA aerogel performed improved catalysis in alkaline, neutral and acidic media as compared to un-doped GA.

Overall, it has been proven that hydrothermal treatment provided opportunities of modulation the final nanomaterial properties regarding its electro-catalytic properties.

Further investigation can be focused on challenge of hydrothermal method in controlling the single nitrogen configuration in N-doped aerogel and more detailed examination of reaction time effect on final composition. Test of CO poisoning and long term stability should be another issue that needs further examination as well as follow up on catalyst ink formation by finding the best ratio between catalyst and binder. There might be prepared optimized GA-N aerogel structures, available for further functionalization in attempt to reach the parameters of Pt/C catalyst and even better.

Závěr

Cílem této diplomové práce byla kontrolovaná hydrotermální syntéza dusíkem dopovaných redukovaných grafenových aerogelů, uskutečněna změnami reakčních podmínek, za účelem získání různých typů dusíku ve finálních nanomateriálech a porovnání jejich elektro-katalytické aktivity pro reakci reduckce kyslíku. Grafen oxid a čtyři dusík-obsahující molekuly (jmenovitě, ethylenedimaine (EDA), *p*-phenylenediamine (pPDA), polyvinylpyrrolidone (PVP) a hydroxid amonný (NH_4OH)) byly použity jako prekurzory.

Detailní charakterizace vzorků potvrdila úspěšnou redukci grafen oxidu na grafenový aerogel a jeho následnou funkcionalizaci dusíkem. Efekt dusíkového dopování se odrazil v rozdílném stupni redukce u jednotlivých nanomateriálů, také v elektrické vodivosti a zlepšeném přenosu elektronů v testovaném redoxním systému. Jako nejvíce elektro-katalyticky aktivní (co se týče hodnot onset potenciálu a proudové hustoty) byl pro redukci kyslíku (ORR) vyhodnocen vzorek GA-N(EDA).

Podmínky ovlivňující syntézu zahrnovaly kromě povahy dusíkového prekurzoru také poměrové množství dusíkového prekurzoru a grafen oxidu (GO:EDA = 1:1, 3:1 and 1:3). Výsledkem této optimalizace byl ovlivněn typ dusíku ve finálních nanomateriálech a stupeň redukce povrchových kyslíkových skupin na původním grafen oxidu. Ze všech čtyř vzorků, použitých na modifikaci rotační diskové elektrody, vzorek GA-N(EDA 3:1) prokázal největší elektro-katalytickou odezvu na ORR.

Vysoce expandovaná struktura a vysoký stupeň redukce vzorku GA-N(EDA 3:1) se odrazila ve vyšším kapacitním proudu a proudové hustotě, zatímco konstituce pyridinického a pyrolického typu dusíku v tomto vzorku se odrazila v největší proudové odezvě v analýze CV a v onset potenciálu katalytické LSV křivky. Pyridinický a pyrolický dusík tedy fungoval jako aktivní promotor v GA-N aerogelech. Tento aerogel navíc v porovnání s nedopovaným aerogelem prokázal zvýšené katalytické vlastnosti v alkalickém, neutrálním i kyselém prostředí.

V souhrnu tedy bylo prokázáno, že hydrotermální metoda umožnila modifikovat vlastnosti finálního nanomateriálu, konkrétně jeho elektro-katalytické vlastnosti.

Další výzkum může být zaměřen na výzvu hydrotermální syntézy v kontrolování jen jednoho konkrétního dusíkového typu v N-GA aerogelu a na detailnější testování efektu reakčního času na finální kompozici nanomateriálu. Testování deaktivace způsobené oxidem uhelnatým, dlouhodobá stabilita a také pokračování v optimalizaci tvorby katalyzátorového filmu, např. poměr katalyzátor-vázač mohou být otázkami dalšího testování. Další výzkum může vést až k přípravě optimalizované GA-N aerogelové struktury, vhodné pro další funkcionalizace, vedoucí k stejným či ještě lepším aktivitám než těm, získaným s Pt/C katalyzátorem.

List of References

1. How Fuel Cells Work | HowStuffWorks. Available at: https://auto.howstuffworks.com/fuel-efficiency/alternative-fuels/fuel-cell.htm. (Accessed: 26th October 2017)

2. Song, C. & Zhang, J. Electrocatalytic oxygen reduction reaction. *PEM fuel cell Electrocatal. Catal. layers* (2008).

3. Shao, M., Chang, Q., Dodelet, J.-P. & Chenitz, R. Recent Advances in Electrocatalysts for Oxygen Reduction Reaction. *Chem. Rev.* **116,** 3594–3657 (2016).

4. Feng, X., Chen, W. & Yan, L. Reduced graphene oxide hydrogel film with a continuous ion transport network for supercapacitors. *Nanoscale* **7,** 3712–3718 (2015).

5. Han, Z. *et al.* Strengthening of graphene aerogels with tunable density and high adsorption capacity towards Pb2+. *Sci. Rep.* **4,** 5025 (2014).

6. Shen, Y., Fang, Q. & Chen, B. Environmental Applications of Three-Dimensional Graphene-Based Macrostructures : Adsorption , Transformation , and Detection. (2015).

7. Eugster, H. P. & Sato, M. Fluid-Mineral Interactions: A Tribute to Thermochemistry of the formation of fossil fuels.

8. Epa, U. & of Resource Conservation, O. *Wastes from the Combustion of Fossil Fuels Report to Congress on Wastes from the Combustion of Fossil Fuels*. (1999).

9. Fossil Fuels | EESI, Environmental and energy study institute. Available at: http://www.eesi.org/topics/fossil-fuels/description. (Accessed: 27th October 2017)

10. European Environment Agency. Available at: https://www.eea.europa.eu/airs/2017/resource-efficiency-and-low-carbon-economy/transport-ghg-emissions. (Accessed: 21st March 2018)

11. Dervisoglu, R. File:Solid oxide fuel cell protonic.svg - Wikimedia Commons. Available at: https://commons.wikimedia.org/wiki/File:Solid_oxide_fuel_cell_protonic.svg. (Accessed: 26th October 2017)

12. KRESTOVÁ, A. Graphene based materials for electrochemical applications. (Palacký University in Olomouc, 2016).

13. Sui, S. *et al.* A comprehensive review of Pt electrocatalysts for the oxygen reduction reaction: Nanostructure, activity, mechanism and carbon support in PEM fuel cells. *J. Mater. Chem. A* **5,** 1808–1825 (2017).

14. Energy Efficiency and Renewable Energy - Hydrogen Storage. Available at: https://www.energy.gov/eere/fuelcells/hydrogen-storage. (Accessed: 10th April 2018)

15. Nie, Y., Li, L. & Wei, Z. Recent advancements in Pt and Pt-free catalysts for oxygen reduction reaction. *Chem. Soc. Rev.* **44,** 2168–2201 (2015).

16. Lv, H. *et al.* Recent advances in the design of tailored nanomaterials for efficient oxygen reduction reaction. (2016). doi:10.1016/j.nanoen.2016.04.008

17. Nørskov, J. K. *et al.* Origin of the overpotential for oxygen reduction at a fuel-cell cathode. *J. Phys. Chem. B* **108,** 17886–17892 (2004).

18. Spiegel, C. Polarization Curves. Available at: http://www.fuelcellstore.com/blog-section/polarization-curves. (Accessed: 7th February 2018)

19. Rotating Electrode Theory – Pine Research Instrumentation Store. Available at: https://www.pineresearch.com/shop/knowledgebase/rotating-electrode-theory/. (Accessed: 25th January 2018)

20. Cyklická voltametrie. doi:10.1017/CBO9781107415324.004

21. BaSi - better data driving better decisions. Available at: https://www.basinc.com/manuals/EC_epsilon/Techniques/CycVolt/cv%0A. (Accessed: 30th April 2018)

22. Lee, S.-J., Pyun, S.-I., Lee, S.-K. & Kang, S.-J. L. Fundamentals of Rotating Disc and Ring-Disc Electrode Techniques and their Applications to Study of the Oxygen Reduction Mechanism at Pt/C Electrode for Fuel Cells. *Isr. J. Chem.* **48,** 215–228 (2008).

23. Town, J. L., Maclaren, F. & Dewald, H. D. Rotating Disk Voltammetry Experiment.

24. Basic Electrochemistry. Available at: https://www.slideshare.net/suey0209/electrochemistry-notes%0A. (Accessed: 24th April 2018)

25. Holton, O. T. & Stevenson, J. W. The Role of Platinum in Proton Exchange Membrane Fuel Cells. *Platin. Met. Rev.* **57,** 259–271 (2013).

26. Schoemaker, M., Misz, U., Beckhaus, P. & Heinzel, A. Evaluation of Hydrogen Crossover through Fuel Cell Membranes. *Fuel Cells* **14,** 412–415 (2014).

27. Krebs, R. E. *The History and Use of Our Earth's Chemical Elements: A Reference Guide, Second Edition*. (Greenwood Press, 2006).

28. Jayaramulu, K. *et al.* Nanoporous Nitrogen-Doped Graphene Oxide/Nickel Sulfide Composite Sheets Derived from a Metal-Organic Framework as an Efficient Electrocatalyst for Hydrogen and Oxygen Evolution. *Adv. Funct. Mater.* **27,** 1–10 (2017).

29. Mahdavi, H., Kahriz, P. K., Gholipour-Ranjbar, H. & Shahalizade, T. Synthesis and performance study of amino functionalized graphene aerogel grafted with polyaniline nanofibers as an efficient supercapacitor material. *J. Mater. Sci. Mater. Electron.* **28,** 4295–4305 (2017).

30. Hu, H., Zhao, Z., Wan, W., Gogotsi, Y. & Qiu, J. Ultralight and Highly Compressible Graphene Aerogels. *Adv. Mater.* **25,** 2219–2223 (2013).

31. Chen, P. *et al.* Hydrothermal synthesis of macroscopic nitrogen-doped graphene hydrogels for ultrafast supercapacitor. *Nano Energy* **2,** 249–256 (2013).

32. Qu, L., Liu, Y., Baek, J.-B. & Dai, L. Nitrogen-Doped Graphene as Efficient Metal-Free Electrocatalyst for Oxygen Reduction in Fuel Cells. *ACS Nano* **4,** 1321–1326 (2010).

33. Allen, M. J., Tung, V. C. & Kaner, R. B. Honeycomb carbon: A review of graphene. *Chem. Rev.* **110,** 132–145 (2010).

34. Geim, A. K. & Novoselov, K. S. The rise of graphene. *Nat. Mater.* **6,** 183–191 (2007).

35. Geim, A. K. Graphene : Status and Prospects. **1530,** 1530–1535 (2010).

36. Georgakilas, V. *Functionalization of Graphene*. (Wiley-VCH Verlag GmbH & Co. KGaA, 2014). doi:10.1002/9783527672790

37. Castro Neto, A. H., Peres, N. M. R., Novoselov, K. S. & Geim, A. K. The electronic properties

of graphene. *Rev. Mod. Phys.* **81,** 109–162 (2009).

38. Georgakilas, V. *et al.* Functionalization of graphene: Covalent and non-covalent approaches, derivatives and applications. *Chem. Rev.* **112,** 6156–6214 (2012).

39. Lee, D. W. *et al.* The structure of graphite oxide: Investigation of its surface chemical groups. *J. Phys. Chem. B* **114,** 5723–5728 (2010).

40. He, H., Klinowski, J., Forster, M. & Lerf, A. A new structural model for graphite oxide. *Chem. Phys. Lett.* **287,** 53–56 (1998).

41. G, W. G. Processable Aqueous Dispersions of Graphene Nanosheets. *Nat. Nanotechnol.* **3,** 101 (2008).

42. Chen, L. *et al.* Influence of Carbon Precursors on the Structure, Composition, and Oxygen Reduction Reaction Performance of Nitrogen-Doped Carbon Materials. *J. Phys. Chem. C* **119,** 28757–28765 (2015).

43. Dimiev, A. M. & Tour, J. M. Mechanism of graphene oxide formation. *ACS Nano* **8,** 3060–3068 (2014).

44. Dreyer, D. R., Park, S., Bielawski, C. W. & Ruoff, R. S. The chemistry of graphene oxide. *Chem. Soc. Rev.* **39,** 228–240 (2010).

45. Zhao, Z. *et al.* One-pot synthesis of lightweight nitrogen-doped graphene hydrogels with supercapacitive properties. *Mater. Res. Bull.* **68,** 245–253 (2015).

46. Zhao, Y. *et al.* A versatile, ultralight, nitrogen-doped graphene framework. *Angew. Chemie - Int. Ed.* **51,** 11371–11375 (2012).

47. Jiang, Y. *et al.* Significant Contribution of Intrinsic Carbon Defects to Oxygen Reduction Activity. *ACS Catal.* **5,** 6707–6712 (2015).

48. Tao, L. *et al.* Edge-rich and dopant-free graphene as a highly efficient metal-free electrocatalyst for the oxygen reduction reaction. *Chem. Commun. Chem. Commun* **52,** 2764–2767 (2764).

49. Sheng, Z.-H. *et al.* Electrochemical sensor based on nitrogen doped graphene: Simultaneous determination of ascorbic acid, dopamine and uric acid. *Biosens. Bioelectron.* **34,** 125–131 (2012).

50. Hao, N. *et al.* AgBr nanoparticles/3D nitrogen-doped graphene hydrogel for fabricating all-solid-state luminol-electrochemiluminescence Escherichia coli aptasensors. *Biosens. Bioelectron.* **97,** 377–383 (2017).

51. Lee, M. S., Choi, H. J., Baek, J. B. & Chang, D. W. Simple solution-based synthesis of pyridinic-rich nitrogen-doped graphene nanoplatelets for supercapacitors. *Appl. Energy* **195,** 1071–1078 (2017).

52. Borghei, M. *et al.* Nitrogen-doped graphene with enhanced oxygen reduction activity produced by pyrolysis of graphene functionalized with imidazole derivatives. *Int. J. Hydrogen Energy* **39,** 12749–12756 (2014).

53. Yadav, R. & Dixit, C. K. Synthesis, characterization and prospective applications of nitrogen-doped graphene: A short review. *J. Sci. Adv. Mater. Devices* **2,** 141–149 (2017).

54. Rani, P. & Jindal, V. K. Designing band gap of graphene by B and N dopant atoms. *RSC Adv.*

3, 802–812 (2013).

55. Panchakarla, L. S. *et al.* Synthesis, structure, and properties of boron- and nitrogen-doped graphene. *Adv. Mater.* **21,** 4726–4730 (2009).

56. Xie, B. *et al.* Hydrothermal synthesis of layered molybdenum sulfide/N-doped graphene hybrid with enhanced supercapacitor performance. *Carbon N. Y.* **99,** 35–42 (2016).

57. Wang, X. *et al.* Heteroatom-doped graphene materials: syntheses, properties and applications. *Chem. Soc. Rev.* **43,** 7067–98 (2014).

58. Woi??ska, M., Milowska, K. & Majewski, J. A. Ab initio modeling of graphene layer functionalized with boron and nitrogen. *AIP Conf. Proc.* **1566,** 143–144 (2013).

59. Zhang, J., Chen, G., Zhang, Q., Kang, F. & You, B. Self-Assembly Synthesis of N-Doped Carbon Aerogels for Supercapacitor and Electrocatalytic Oxygen Reduction. *ACS Appl. Mater. Interfaces* **7,** 12760–12766 (2015).

60. Tian, G.-L. *et al.* Nitrogen-Doped Graphene/Carbon Nanotube Hybrids: In Situ Formation on Bifunctional Catalysts and Their Superior Electrocatalytic Activity for Oxygen Evolution/Reduction Reaction. *Small* **10,** 2251–2259 (2014).

61. Guo, D. *et al.* Active sites of nitrogen-doped carbon materials for oxygen reduction reaction clarified using model catalysts. *Science* **351,** 361–5 (2016).

62. Soo, L. T., Loh, K. S., Mohamad, A. B., Daud, W. R. W. & Wong, W. Y. Effect of nitrogen precursors on the electrochemical performance of nitrogen-doped reduced graphene oxide towards oxygen reduction reaction. *J. Alloys Compd.* **677,** 112–120 (2016).

63. Hassan, F. M. *et al.* Pyrrolic-structure enriched nitrogen doped graphene for highly efficient next generation supercapacitors. *J. Mater. Chem. A* **1,** 2904 (2013).

64. Jiang, X., Ma, Y., Li, J., Fan, Q. & Huang, W. Self-Assembly of Reduced Graphene Oxide into Three-Dimensional Architecture by Divalent Ion Linkage. *J. Phys. Chem. C* **114,** 22462–22465 (2010).

65. Dong, H. *et al.* Three-dimensional Nitrogen-Doped Graphene Supported Molybdenum Disulfide Nanoparticles as an Advanced Catalyst for Hydrogen Evolution Reaction. *Sci. Rep.* **5,** 17542 (2015).

66. Qu, L., Liu, Y., Baek, J. B. & Dai, L. Nitrogen-doped graphene as efficient metal-free electrocatalyst for oxygen reduction in fuel cells. *ACS Nano* **4,** 1321–1326 (2010).

67. Yang, Y. *et al.* A biomass derived N/C-catalyst for the electrochemical production of hydrogen peroxide. *Chem. Commun. Chem. Commun* **9994,** 9994–9997 (2017).

68. Panchakarla, L. S. *et al.* Synthesis, Structure and Properties of Boron and Nitrogen Doped Graphene. 12 (2009). doi:10.1002/adma.200901285

69. Ying, Z. C., Hettich, R. L., Compton, R. N. & Haufler, R. E. Synthesis of nitrogen-doped fullerenes by laser ablation. *J. Phys. B At. Mol. Opt. Phys.* **29,** 4935–4942 (1996).

70. Lai, L. *et al.* Exploration of the active center structure of nitrogen-doped graphene-based catalysts for oxygen reduction reaction. *Energy Environ. Sci.* **5,** 7936 (2012).

71. Mou, Z. *et al.* Forming mechanism of nitrogen doped graphene prepared by thermal solid-state reaction of graphite oxide and urea. *Appl. Surf. Sci.* **258,** 1704–1710 (2011).

72. Li, S. M. *et al.* Controllable synthesis of nitrogen-doped graphene and its effect on the simultaneous electrochemical determination of ascorbic acid, dopamine, and uric acid. *Carbon N. Y.* **59,** 418–429 (2013).

73. Han, Z. *et al.* Strengthening of graphene aerogels with tunable density and high adsorption capacity towards Pb2+. *Sci. Rep.* **4,** 5025 (2014).

74. Guo, D. *et al.* Active sites of nitrogen-doped carbon materials for oxygen reduction reaction clarified using model catalysts. *Science* **351,** 361–5 (2016).

75. Xu, Y. *et al.* Solvated graphene frameworks as high-performance anodes for lithium-ion batteries. *Angew. Chem. Int. Ed. Engl.* **54,** 5345–50 (2015).

76. Zhang, J. *et al.* 3D free-standing nitrogen-doped reduced graphene oxide aerogel as anode material for sodium ion batteries with enhanced sodium storage. *Sci. Rep.* **7,** 4886 (2017).

77. Liu, Y. *et al.* Exploring the nitrogen species of nitrogen doped graphene as electrocatalysts for oxygen reduction reaction in Al-air batteries. *Int. J. Hydrogen Energy* **41,** 10354–10365 (2016).

78. Megawati, M., Chua, C. K., Sofer, Z., Klímová, K. & Pumera, M. Nitrogen-doped graphene: Effect of graphite oxide precursors and nitrogen content on the electrochemical sensing properties. *Phys. Chem. Chem. Phys.* **19,** 15914–15923 (2017).

79. Men, B. *et al.* Hierarchical Metal-Free Nitrogen-Doped Porous Graphene/Carbon Composites as an Efficient Oxygen Reduction Reaction Catalyst. *ACS Appl. Mater. Interfaces* **8,** 1415–1423 (2016).

80. Liao, Y. *et al.* Three-dimensional nitrogen-doped graphene hydrogels prepared via hydrothermal synthesis as high-performance supercapacitor materials. *Electrochim. Acta* **194,** 136–142 (2016).

81. Li, Y. *et al.* Building three-dimensional porous nano-network for the improvement of iron and nitrogen-doped carbon oxygen reduction electrocatalyst. (2017). doi:10.1016/j.carbon.2017.09.106

82. Kang, B. K. *et al.* Synthesis and characterization of a mesoporous and three dimensional N-doped graphene structure via the Couette-Taylor flow and hydrothermal method. *J. Eur. Ceram. Soc.* **37,** 3673–3680 (2017).

83. Luo, Z. *et al.* Pyridinic N doped graphene: synthesis, electronic structure, and electrocatalytic property. *J. Mater. Chem.* **21,** 8038 (2011).

84. Schiros, T. *et al.* Connecting Dopant Bond Type with Electronic Structure in N-Doped Graphene. *Nano Lett.* **12,** 4025–4031 (2012).

85. Zhang, Y. *et al.* Manageable N-doped Graphene for High Performance Oxygen Reduction Reaction. *Sci. Rep.* **3,** 2771 (2013).

86. Yasuda, S., Yu, L., Kim, J. & Murakoshi, K. Selective nitrogen doping in graphene for oxygen reduction reactions. *Chem. Commun. Chem. Commun* **49,** 9627–9629 (2013).

87. Zhang, L. & Xia, Z. Mechanisms of Oxygen Reduction Reaction on Nitrogen-Doped Graphene for Fuel Cells. *J. Phys. Chem. C* **115,** 11170–11176 (2011).

88. Ambrosi, A. *et al.* Graphene and its electrochemistry – an update. *Chem. Soc. Rev.* **45,** 2458–2493 (2016).

89. Wu, P., Qian, Y., Du, P., Zhang, H. & Cai, C. Facile synthesis of nitrogen-doped graphene for measuring the releasing process of hydrogen peroxide from living cells. *J. Mater. Chem.* **22,** 6402 (2012).

90. Lee, M. S. *et al.* A facile approach to tailoring electrocatalytic activities of imine-rich nitrogen-doped graphene for oxygen reduction reaction. (2017). doi:10.1016/j.carbon.2017.07.001

91. Marcano, D. C. *et al.* Improved Synthesis of Graphene Oxide. *ACS Nano* **4,** 4806–4814 (2010).

92. Wu, L. Facile Synthesis of 3D Amino-Functional Graphene-Sponge Composites Decorated by Graphene Nanodots with Enhanced Removal of Indoor Formaldehyde. *Aerosol Air Qual. Res.* **2015,** (2015).

93. Leng, Y. *Materials characterization: introduction to microscopic and spectroscopic methods*. (Weinheim, Wiley VCH, 2013).

94. Dresselhaus, M. S., Jorio, A. & Saito, R. Characterizing Graphene, Graphite, and Carbon Nanotubes by Raman Spectroscopy. *Annu. Rev. Condens. Matter Phys* **1,** 89–108 (2010).

95. Jiang, Z., Jiang, Z., Tian, X. & Chen, W. Amine-functionalized holey graphene as a highly active metal-free catalyst for the oxygen reduction reaction. *J. Mater. Chem. A* **2,** 441–450 (2014).

96. Tripathi, P., Patel, C. R. P., Shaz, M. A. & Srivastava, O. N. Synthesis of High-Quality Graphene through Electrochemical Exfoliation of Graphite in Alkaline Electrolyte. 15 (2013).

97. Sun, L. *et al.* Nitrogen-doped graphene with high nitrogen level via a one-step hydrothermal reaction of graphene oxide with urea for superior capacitive energy storage. *RSC Adv.* **2,** 4498 (2012).

98. Zafar, Z. *et al.* Evolution of Raman spectra in nitrogen doped graphene. *Carbon N. Y.* **61,** 57–62 (2013).

99. Samadaei, F., Salami-Kalajahi, M., Roghani-Mamaqani, H. & Banaei, M. A structural study on ethylenediamine- and poly(amidoamine)-functionalized graphene oxide: simultaneous reduction, functionalization, and formation of 3D structure. *RSC Adv.* **5,** 71835–71843 (2015).